JGR Planets

RESEARCH ARTICLE
10.1029/2022JE007516

Special Section:
The Mars Perseverance Rover Jezero Crater Floor Campaign

Convective Vortices and Dust Devils Detected and Characterized by Mars 2020

R. Hueso[1], C. E. Newman[2], T. del Río-Gaztelurrutia[1], A. Munguira[1], A. Sánchez-Lavega[1], D. Toledo[3], V. Apéstigue[3], I. Arruego[3], A. Vicente-Retortillo[4], G. Martínez[5], M. Lemmon[6], R. Lorenz[7], M. Richardson[2], D. Viudez-Moreiras[4], M. de la Torre-Juarez[8], J. A. Rodríguez-Manfredi[4], L. K. Tamppari[8], N. Murdoch[9], S. Navarro-López[4], J. Gómez-Elvira[4], M. Baker[10], J. Pla-García[4], A. M. Harri[11], M. Hieta[11], M. Genzer[11], J. Polkko[11], I. Jaakonaho[11], T. Makinen[11], A. Stott[9], D. Mimoun[9], B. Chide[12], E. Sebastian[4], D. Banfield[13], and A. Lepinette-Malvite[4]

[1]Física Aplicada, Escuela de Ingeniería de Bilbao, Universidad del País Vasco UPV/EHU, Bilbao, Spain, [2]Aeolis Research, Chandler, AZ, USA, [3]Instituto Nacional de Técnica Aeroespacial (INTA), Madrid, Spain, [4]Centro de Astrobiología (INTA-CSIC), Madrid, Spain, [5]Lunar and Planetary Institute, Houston, TX, USA, [6]Space Science Institute, College Station, TX, USA, [7]Johns Hopkins Applied Physics Laboratory, Laurel, MD, USA, [8]Jet Propulsion Laboratory/California Institute of Technology, Pasadena, CA, USA, [9]Institut Supérieur de l'Aéronautique et de l'Espace (ISAE-SUPAERO), Université de Toulouse, Toulouse, France, [10]Smithsonian Institution, Washington, DC, USA, [11]Finnish Meteorological Institute, Helsinki, Finland, [12]Los Alamos National Laboratory, Los Alamos, NM, USA, [13]Cornell Center for Astrophysics and Planetary Science, Cornell University, Ithaca, NY, USA

Key Points:

- Vortices and dust devils (DDs) are frequent on Jezero. Mars Environmental Dynamics Analyzer detects 5.0 and 1.0 events per sol respectively when correcting from sampling effects
- Intense vortices on Jezero tend to be dusty with 75% of all vortices with a pressure drop larger than 2.0 Pa being dusty
- We calculate 2.5 and 0.1 DDs $km^{-2}sol^{-1}$ with sizes of 20 and 100 m respectively. The largest events dominate dust lifting

Supporting Information:

Supporting Information may be found in the online version of this article.

Correspondence to:

R. Hueso,
Ricardo.Hueso@ehu.eus

Citation:

Hueso, R., Newman, C. E., del Río-Gaztelurrutia, T., Munguira, A., Sánchez-Lavega, A., Toledo, D., et al. (2023). Convective vortices and dust devils detected and characterized by Mars 2020. *Journal of Geophysical Research: Planets*, *128*, e2022JE007516. https://doi.org/10.1029/2022JE007516

Received 3 AUG 2022
Accepted 22 NOV 2022

Author Contributions:

Conceptualization: R. Hueso, C. E. Newman, D. Toledo, V. Apéstigue, I. Arruego, A. Vicente-Retortillo, G. Martínez
Data curation: R. Hueso, C. E. Newman, G. Martínez, M. Lemmon

Abstract We characterize vortex and dust devils (DDs) at Jezero from pressure and winds obtained with the Mars Environmental Dynamics Analyzer (MEDA) instrument on Mars 2020 over 415 Martian days (sols) ($Ls = 6°–213°$). Vortices are abundant (4.9 per sol with pressure drops >0.5 Pa correcting from gaps in coverage) and they peak at noon. At least one in every five vortices carries dust, and 75% of all vortices with $\Delta p > 2.0$ Pa are dusty. Seasonal variability was small but DDs were abundant during a dust storm ($Ls = 152°–156°$). Vortices are more frequent and intense over terrains with lower thermal inertia favoring high daytime surface-to-air temperature gradients. We fit measurements of winds and pressure during DD encounters to models of vortices. We obtain vortex diameters that range from 5 to 135 m with a mean of 20 m, and from the frequency of close encounters we estimate a DD activity of 2.0–3.0 DDs km^{-2} sol^{-1}. A comparison of MEDA observations with a Large Eddy Simulation of Jezero at $Ls = 45°$ produces a similar result. Three 100-m size DDs passed within 30 m of the rover from what we estimate that the activity of DDs with diameters >100 m is 0.1 DDs $km^{-2}sol^{-1}$, implying that dust lifting is dominated by the largest vortices in Jezero. At least one vortex had a central pressure drop of 9.0 Pa and internal winds of 25 ms^{-1}. The MEDA wind sensors were partially damaged during two DD encounters whose characteristics we elaborate in detail.

Plain Language Summary Dust devils (DDs) are whirlwinds of warm air with winds strong enough to lift dust. They are common in Earth deserts and much more abundant on Mars, where they are one of the elements that bring dust to the atmosphere. The Mars 2020 mission landed in Jezero crater on February 2020 and has observed a plethora of DDs that we investigate with the meteorological sensors on the Mars Environmental Dynamics Analyzer (MEDA) instrument. Results for more than 400 Martian days from spring to autumn indicate a high abundance of events with small seasonal variability. Terrains with lower thermal inertia, warming more efficiently at noon, favor the appearance of DDs. We also found an increased DD activity during a short dust storm that covered the region. From modeling MEDA data, we find that DDs at Jezero have diameters from 5.0 to 135 m. We estimate that about 2–3 DDs are formed per km^2 and Martian day. Large vortices with diameters of 100 m form frequently enough to dominate dust lifting at Jezero. Two DDs damaged part of the hardware of the wind sensors of MEDA and we detail the characteristics of those events.

1. Introduction

Daytime convective vortices are common on Mars and Earth (Balme & Greeley, 2006). They constitute one of the various phenomena that develop in the Planetary Boundary Layer (PBL) of both planets, but are much more common and can be an order of magnitude larger on Mars due to the more extended PBL depth (Balme & Greeley, 2006). Dusty convective vortices, or dust devils (DDs), are vortices that have raised dust from the

Formal analysis: R. Hueso, T. del Río-Gaztelurrutia, A. Munguira, A. Sánchez-Lavega
Funding acquisition: A. Sánchez-Lavega
Investigation: R. Hueso
Writing – original draft: R. Hueso
Writing – review & editing: R. Hueso, C. E. Newman, T. del Río-Gaztelurrutia, A. Munguira, A. Sánchez-Lavega, D. Toledo, V. Apéstigue, I. Arruego, A. Vicente-Retortillo, G. Martínez, M. Lemmon, R. Lorenz, M. Richardson, D. Viudez-Moreiras, M. de la Torre-Juarez, J. A. Rodríguez-Manfredi, L. K. Tamppari, N. Murdoch, S. Navarro-López, J. Gómez-Elvira, M. Baker, J. Pla-García, A. M. Harri, M. Hieta, M. Genzer, J. Polkko, I. Jaakonaho, T. Makinen, A. Stott, D. Mimoun, B. Chide, E. Sebastian, D. Banfield, A. Lepinette-Malvite

surface, via the combination of tangential winds around the vortex, central pressure drop, and electrostatic forces between dust grains (Neakrase et al., 2016). DDs constitute an important element of the Martian atmospheric dust cycle thought to account for a significant part of the background dust haze on Mars (Basu et al., 2004; Kahre et al., 2006, 2017; Newman et al., 2002). In addition, DDs can change the local albedo creating Dust Devil Tracks that can affect large-scale weather patterns (Fenton et al., 2016; Reiss et al., 2016). DDs can also "clean" dust off spacecraft surfaces (Vicente-Retortillo et al., 2018), including solar panels (R. D. Lorenz & Reiss, 2015), enabling solar-powered missions to last longer. Conversely, dust grains carried by the strong vortex winds can represent a hazard to surface hardware (Balme & Greeley, 2006). Thus, characterizing the DD activity at Jezero, the location of the Mars 2020 mission, which is collecting the first samples of Mars to be brought to Earth (Farley et al., 2020), is important for understanding the specific risks to the landed elements involved in the Mars Sample Return mission.

Field data obtained by meteorological sensors can characterize the physical properties of convective vortices and imaging instruments can also determine many of the properties of DDs (Murphy et al., 2016). Vortices can be identified by dips in the pressure record and in sharp changes in wind intensity and direction (Ryan & Lucich, 1983). Vortices also produce warmer temperatures at their core, and the presence of dust can be investigated with photodiodes (Kahanpää & Viúdez-Moreiras, 2021; Mason et al., 2013; Ordóñez-Etxeberria et al., 2020).

The Mars Environmental Dynamics Analyzer (MEDA) instrument on the Mars 2020 Perseverance rover carries sensors capable of simultaneously obtaining all those measurements (Rodriguez-Manfredi et al., 2021). MEDA measures air pressure and horizontal winds that can be used to determine the physical properties of the vortices. The Radiation and Dust Sensors (RDSs) on MEDA are a set of photodiodes oriented at different directions including a panchromatic sensor pointing to the vertical (RDS Top 7) with a 90° Field of View (Apestigue et al., 2022). In addition, MEDA measures the ground and air temperatures at different altitudes using the Thermal InfraRed Sensors (TIRSs) and Air Temperature Sensors (ATSs) packages (Munguira et al., 2023; Rodriguez-Manfredi et al., 2021, 2023), therefore, obtaining the near surface temperature lapse rate, which is a key element in determining the frequency, intensity, horizontal size, and vertical extension of the vortices (Ordóñez-Etxeberria et al., 2020; Rennó et al., 1998; Ryan, 1972; Spiga et al., 2021). Thus, multi-sensorial investigations of convective vortices and DDs, and the properties of the environment in which they develop are possible with MEDA.

The Mars 2020 Perseverance rover landed on Mars in Jezero crater at 77.5°E and 18.4°N at $Ls = 6.2°$ (North hemisphere Spring) on Martian Year 36 (MY36). Predictions before landing based on the Mars atmospheric models suggested that Jezero is a location where intense vortices form regularly, peaking in activity at $Ls \sim 120°$ (Newman et al., 2021). Jackson (2022b) performed an initial analysis of MEDA pressure and RDS data in the first 89 sols of the mission, finding a high frequency of vortices and high rate of DDs. In a later study, Jackson (2022a) examined temperatures during passage of vortices during the first 179 sols of the mission to examine the thermodynamics and estimate possible heights of vortices on Jezero. A more extensive analysis by Newman et al. (2022) up to mission sol 216 (covering early spring through early summer) examined vortices, DDs, and winds in MEDA data comparing with results from the Mars 2020 imaging instruments. Newman et al. (2022) found that on average, over four vortices passed the rover per sol with at least a quarter of which were dusty, and with dust lifting in Jezero caused by both DDs and large wind gusts associated to convective cells. Newman et al. (2022) also found a positive correlation between vortex intensity (in terms of the measured pressure drop and wind speed) and dust lifting (in terms of vortex dust content and local surface dust removal).

The abundance of DDs at Jezero has a stark contrast with the lack of them in Elysium Planitia, where the InSight mission has detected thousands of vortices (Banfield et al., 2020; Chatain et al., 2021; Jackson et al., 2021; Spiga et al., 2021) with no dust activity (R. D. Lorenz et al., 2021). Following arguments presented by Spiga et al. (2021) of vortex abundance being influenced by environment winds, Newman et al. (2022) concluded that the intrinsic activity of vortices at Elysium Planitia and Jezero is very similar over spring and early summer, but the stronger winds at Elysium advected vortices more rapidly over the sensors, resulting in nearly double the number of detections. Differences in the DD abundance are most likely due to distinct surface properties, including the different availability at the surface of mobile dust particles.

Here we extend the vortex and DD results presented in Newman et al. (2022) to cover the first 415 sols of the mission from $Ls = 6°$ (northern hemisphere spring) to $Ls = 213°$ (northern hemisphere autumn). This allows us to explore the effects on the vortex and DD activity caused by the combination of seasonal variations and changes

in the properties of the terrain traversed by Perseverance. In addition, we study the effect on vortices and DDs of a regional dust storm that covered Jezero on $Ls = 153°–156°$ (Mars 2020 sols 312–318), which significantly affected the local environment (Lemmon et al., 2022). Further insights can be gained through comparisons with models of vortices, simulations of the convective activity at Jezero from a Large Eddy Simulation (LES) and statistical analysis of the closest DD approaches to Perseverance resulting in estimates of the density of DDs in Jezero. Our results are summarized in a catalog of convective vortex encounters through sol 415 of the mission. The catalog summarizes properties such as the duration and magnitude of the pressure excursion, detection of dust or not, and thermal properties of the environment during the event. The catalog is complemented by a larger catalog of pressure drops containing additional long and turbulent events, physical parameters of a selection of vortices, and DDs from model fits and a movie of the LES, all available online (Hueso et al., 2022).

The structure of this paper is as follows. Section 2 describes MEDA data sets and the analyses conducted to identify vortices and DDs, the results of which are shown in Section 3. Section 4 describes the variability of this activity, including its seasonal evolution, variations associated with the dust storm, and effects linked to different terrains. Section 5 presents a more detailed analysis of a subset of DDs obtained by fitting the observed pressure and winds to a model of a drifting vortex. Section 6 explores a comparison of our in situ data with a LES of vortex activity at Jezero. Section 7 discusses the density of DDs in Jezero and gives details of two DDs that partially damaged MEDA wind sensors (WSs). Section 8 presents a summary of our conclusions. Times in this paper are given in terms of Local True Solar Time (LTST).

2. Data and Data Analysis

MEDA acquires data in measurement sessions that can extend from 5 min to a few hours and that typically cover 54% of a sol. The data is obtained with a cadence of 1 Hz in most sensors (including pressure), and up to 2 Hz in the five Atmospheric Temperature Sensors (ATSs) and the two WSs. Gaps in the data are due to a combination of minor hardware issues and mission operations. The WSs were required to be off during orbiter communication passes, and as a result, some observed vortex encounters do not have simultaneous wind data. In addition, one of the two WSs was partially damaged on sol 313 by a DD that will be described in Section 7. Wind data obtained afterward requires modified wind retrievals which were not yet available at the time of writing this paper. Figure S1 in Supporting Information S1 shows the cadence of MEDA observations. About 64% of all vortices detected in the pressure field have simultaneous wind data.

2.1. Vortex Detection

We search the entire pressure data set for vortex pressure drops by using a moving window of a fixed time duration. We use a linear fit to the first and last 10% of the pressure signal disregarding the central 80%. The pressure minus the linear fit form a signal detrended from the daily variation of pressure. When the central point of the detrended signal is at least −0.3 Pa, we identify a candidate vortex event and plot the pressure for the event together with a Gaussian and Lorentzian fit to quantify the duration of the event (Ellehoj et al., 2010). The moving window advances by 1 s on each evaluation scanning the whole MEDA pressure data set. We perform several searches of the data with time windows of 80 and 190 s with a detection threshold of 0.3 Pa and searches with a time window of 60, 120, 180, 300, 600, and 900 s with a detection threshold of 0.5 Pa. This dual strategy is based on both the sensor noise level (∼0.04 Pa, see Sánchez-Lavega et al., 2022) and experiments with the data. Detection thresholds from 0.3 to 0.5 Pa with long time windows produce numerous false detections caused by small-scale fluctuations of pressure. However, there are many short-duration vortices with pressure dips in the 0.3–0.5 Pa range. Figure S2 in Supporting Information S1 shows the cumulative distribution in terms of Δp of pressure drops with a shape characteristic of the passage of a vortex. Power law fits to this distribution have similar slopes for different ranges of Δp, which is a good indication that the survey is complete for pressure dips larger than 0.5 Pa.

Figure 1 shows examples of typical vortices found on a single sol, and demonstrates how different time windows are needed to identify and quantify the properties of very different events. Fitting a vortex with a Gaussian function or a Lorentzian results in slightly different values of the intensity of the pressure drop and its duration. Typically these parameters can vary up to 12% in Δp, and up to 25% in the duration of the event. Lorentzian functions generally fit better in the central part of the encounter, while Gaussians can fit better in the approach and distance phases. Vortices not moving with a constant velocity produce more complex patterns not well fit by these functions (R. Lorenz, 2013; R. D. Lorenz, 2013).

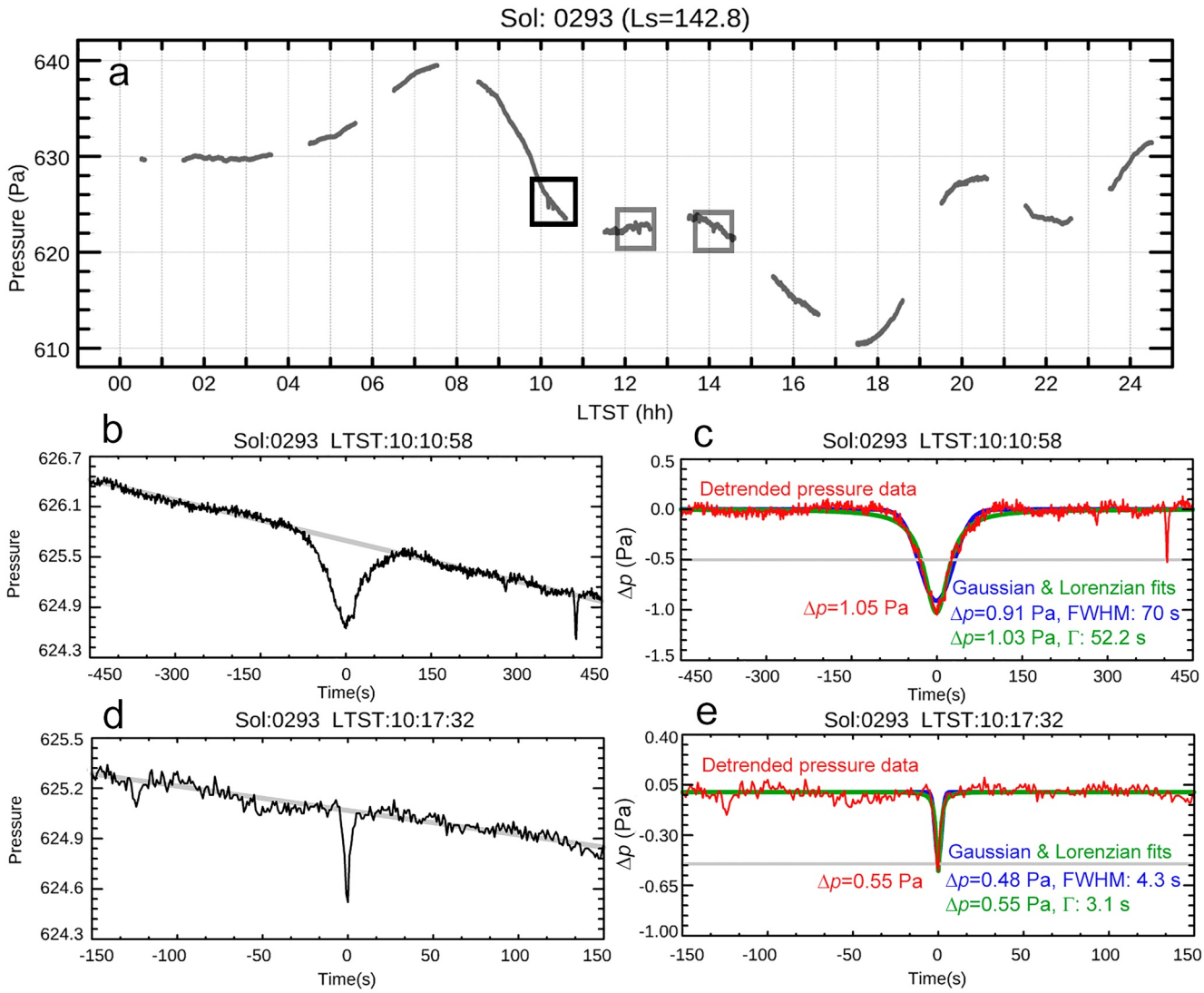

Figure 1. Finding vortices in Mars Environmental Dynamics Analyzer data. (a) Pressure over sol 293. Boxes identify the location of four vortices. (b) Two typical vortices. The second one is invisible to the algorithm operating over long time windows. (c) Vortex fitting for the first event in panel (b). Detrended data (red) compared with a Gaussian fit (blue) and a Lorentzian function (green) with similar parameters defining each fit. (d) Second vortex identified using a short time window. (e) Vortex fitting for the event in panel (d).

Each evaluation of the algorithm generates a catalog of events and a series of plots that are visually examined to remove spurious and duplicate detections and select the time window that results in the best fit to each event. This selection generally considers the longest time window in which the vortex is well-fit and in which additional vortices like those seen in Figure 1b do not influence the fit. The 300 s time window is found to capture the majority of events, but shorter time windows provide better fits to short or weak events, and long time windows can be required in some cases for a good fit to the data. The longest time windows also allow the detection of longer pressure drops that do not fit a vortex signature, but are instead possibly related to the passage of the low-pressure edges of convective cells. An event of this type is the gust wind event on sol 117 described by Newman et al. (2022) that was associated with a large dust lifting event.

2.2. Vortex Characterization

For each event, we generate plots of all MEDA sensors using a time window of 8 min. These plots are examined to quantify the properties of each pressure drop, such as the simultaneous detection of a change in airborne dust from RDS Top 7. We also examine changes in wind speed and direction, and the thermal response of the surface

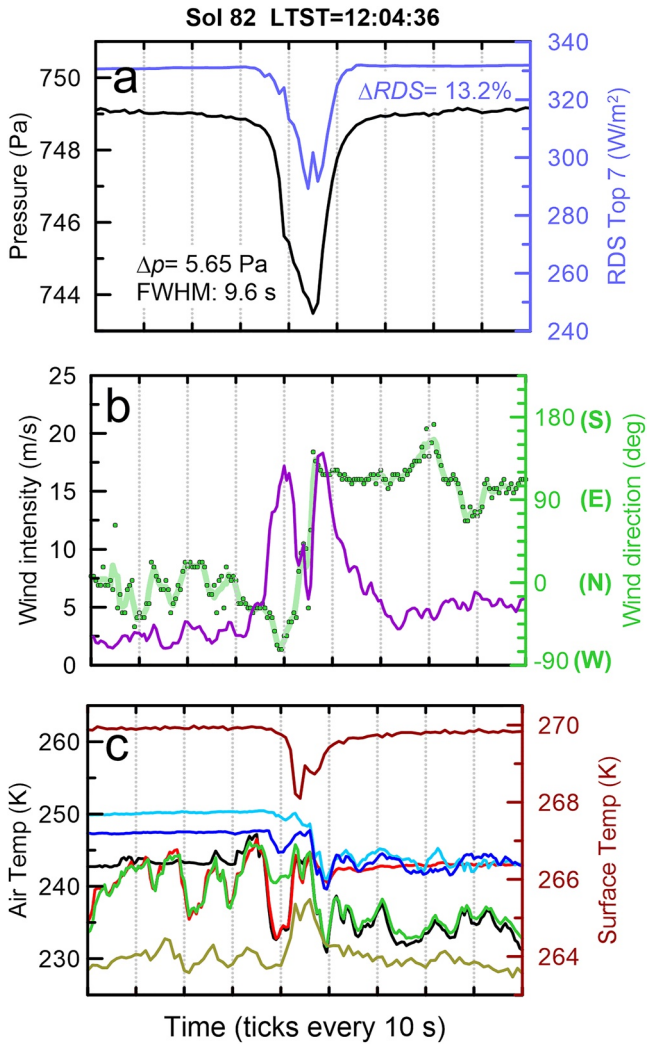

Figure 2. Dust devil on sol 82. (a) Pressure (black line, left axis) and solar irradiance from Radiation and Dust Sensor (RDS) Top 7 (blue line, right axis). (b) Wind speeds (purple line, left axis) and direction from which the wind is coming (green line and symbols, right axis). (c) Temperatures during the vortex passage. From top to bottom: Surface temperature (dark-red, right axis); air temperature at $z = 0.85$ m from ATS5 (cyan) and ATS4 (dark blue), located at the front of the rover; air temperature at $z = 1.45$ m from ATS1 (black), ATS2 (red), and ATS3 (green) located around the Remote Sensing Mast; air temperature at $z \sim 40$ m (green-yellow) from Thermal InfraRed Sensor channel 2. Note the strong thermal gradient of 40 K from the surface to 40 m during this event and the change in wind direction and thermal behavior of the different Air Temperature Sensor after the vortex passage.

and the atmosphere to the passage of the vortex. Variations in the lateral RDS detectors can be found both during and outside of the pressure drops, and are caused by vortices passing at a range of distances from very close to the rover up to 1 km. Vortices found in the RDS lateral detectors are not examined in this work and are the subject of a parallel analysis (Toledo et al., 2023).

Figure 2 shows an example of the multi-sensorial response of the atmosphere to the passage of a strong convective DD. The vortex produced a pressure drop of 5.7 Pa with a Full Width at Half Maximum (FWHM) duration of 9.6 s from the Gaussian fit. The dust in this event resulted in a decrease of the RDS Top 7 signal of 13%, with additional counterparts in RDS lateral sensors (not shown here). This corresponds to an increase of the optical depth of $\Delta\tau = 0.14$, which can be compared with values of optical depths at Jezero over that period of 0.4–0.5 (Rodriguez-Manfredi et al., 2023). MEDA measured winds of 18 ms^{-1} distributed in two peaks coincident in time with half the maximum pressure drop. This symmetric double peak wind structure and its timing with respect to the pressure drop indicate a direct encounter with a vortex, in which each peak in the winds corresponds to the maximum winds in the "walls" of the vortex as it approaches and recedes from Perseverance. This is confirmed from fitting the pressure and wind data from this vortex to models of passing vortices in Section 5. The direct encounter implies that at the central time we are measuring the physical properties of the center of the vortex and that vortices and DDs in Jezero are common enough to produce extremely close encounters, an aspect we discuss in Section 7.

Figure 2c focuses on the complex measurements of temperatures during this event. At the time of this event the rover orientation and ambient wind direction were such that air warmed by the Perseverance's Radio-isotope Thermonuclear Generator (RTG), situated at the rover's rear, was carried over the ATS, creating an increased level of thermal fluctuations (Munguira et al., 2023). With the vortex arrival, the winds bring air not exposed to the RTG, reducing the thermal fluctuations to typical levels during the convective period. Our assessment of the thermal plume associated to the vortex from ATS measurements at $z = 1.45$ m, based on the change in ATS measurements during the central part of the vortex passage compared with the later ATS measurements obtained after a change of winds without RTG perturbations, is +8 K. This estimate is a best guess that agrees with similar observations of other vortices, and constitutes more of an upper limit to the increase of temperatures during the vortex passage than a real measurement of the inner temperatures in the vortex. Thermal effects of the vortex at $z = 0.85$ m cannot be quantified for this event, as both sensors are located in the front of the rover and are sheltered from the wind before and after the vortex arrival. Air temperatures obtained by the TIRS instrument at an approximate altitude of $z \sim 40$ m are not affected by the thermal influence of the RTG and show an increase of temperatures during the vortex passage of +9 K, giving further support to the estimate of temperature effects given above. The ground-surface temperatures, also measured by TIRS, experiences a short cooling of −1.8 K during the vortex passage followed by a gradual recovery of temperatures. This example shows that the measurement of the internal thermal structure of vortices is complex and we leave for future work a thermodynamic characterization of a selection of the best cases. The analysis of temperatures measured by MEDA in vortices at Jezero by Jackson (2022a), which is based in the ATS sensor that is best correlated with the pressure data during a vortex event, is a simplified version of the true process, in which winds changing in direction as the vortex passes, suggest a more sophisticated analysis. On the other hand, the capability to measure the surface-to-air temperature difference at the time of MEDA vortices is an important piece of information that we will examine in Section 4.

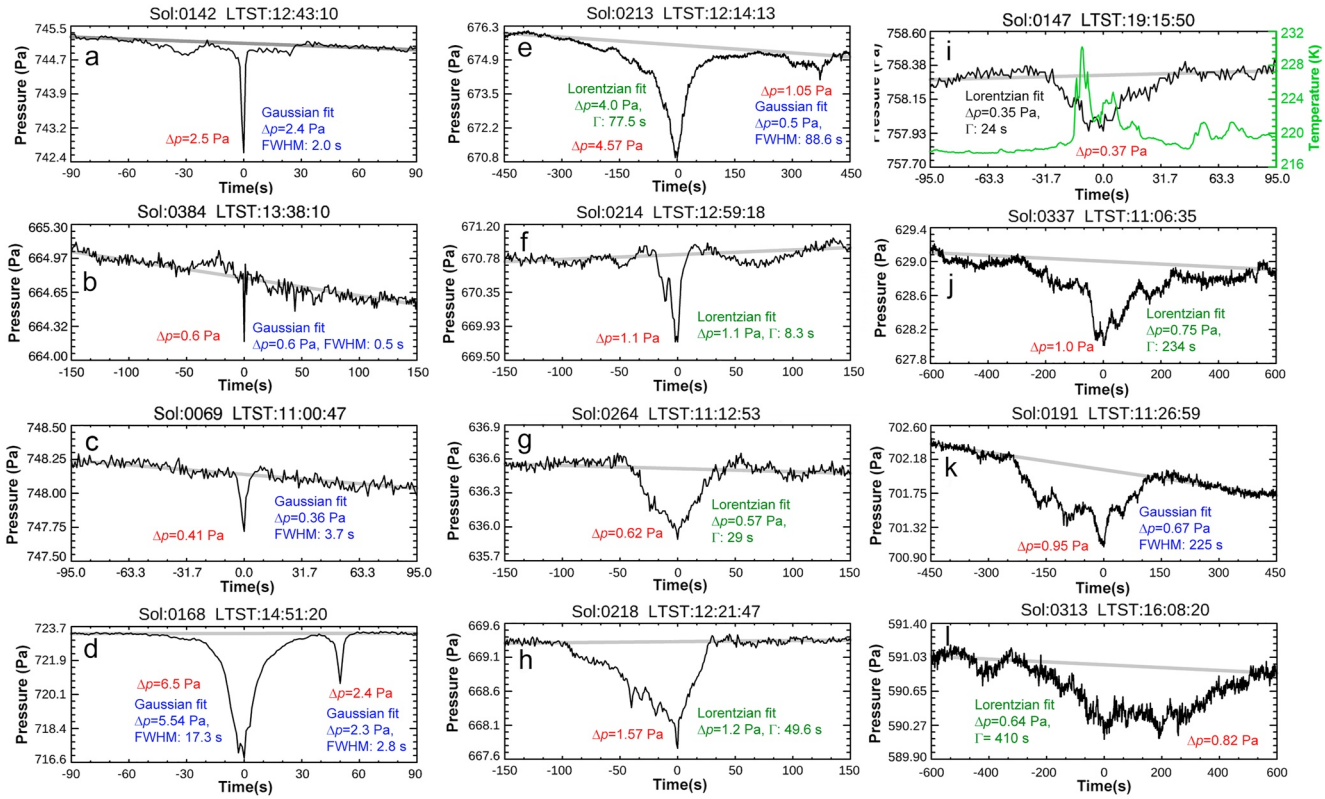

Figure 3. Variety of pressure drops on Jezero (a–e): Typical vortices. (f) Double event (g and h) Events with pressure profiles suggesting more distant passages of vortices. (i) Long pressure drop during the night accompanied by a thermal plume originated over the RTG (right-axis). (j–l) Long duration events with turbulent fluctuations that transition from a vortex behavior embedded in a larger structure of pressure drop (j) to turbulent pressure drops (k–l) not considered as vortices.

3. Pressure Drops: Vortices, Dust Devils, Convective Cells, and Waves

3.1. Catalog of Pressure Drops

Our survey of pressure drops shows events with varied characteristics, and their classification requires a visual examination of the pressure drops and related environmental variables.

Figure 3 shows examples of pressure curves associated with different types of events. Besides standard cases (a), in which a narrow and intense pressure drop marks the close passage of a vortex, vortices can be short (b), weak (c), intense and short (d), or intense and long (e). Double vortices or very close events are also detected (f). Long pressure drops can have more flat profiles with inner structure (g and h). Some of the nighttime vortex-like pressure drops are coincident with turbulent pulses of high-temperatures measured with the ATS. These events are most likely caused by weak winds flowing above the rover's RTG (Figure 3i), and thus, are similar to the nighttime vortices found by the Viking Lander, which were attributed to the Lander acting as a heat island Ryan and Lucich (1983). MEDA data allows us to demonstrate the artificial nature of some of these events thanks to wind measurements showing the direction of the winds coming from the RTG position at the back of the rover toward the front of Perseverance. Other nighttime pressure dips equivalent in shape to those caused by daytime vortices, are found in the data with winds coming from the opposite direction of the RTG, with no clear thermal counterparts, and are equivalent to other nighttime pressure drops found in other Martian locations and suggestive of turbulence. Nighttime pressure drops can be driven by orographic mechanical turbulence at Gale crater (Ordonez-Etxeberria et al., 2018), and by the interaction of a low-level jet and weak stability in Elysium (Chatain et al., 2021). In Jezero, nighttime turbulence appears in different atmospheric fields (winds, pressure and temperature) and has the characteristics of a bore-like disturbance (Pla-Garcia et al., 2022) that could be the cause of the nighttime pressure drops not associated to the heat island effect.

Another type of event consists of long and turbulent pressure drops, typically observed near noon, which sometimes exceed durations of 200–300 s Figures 3k–3l. Some of these can be interpreted as the passing of convective

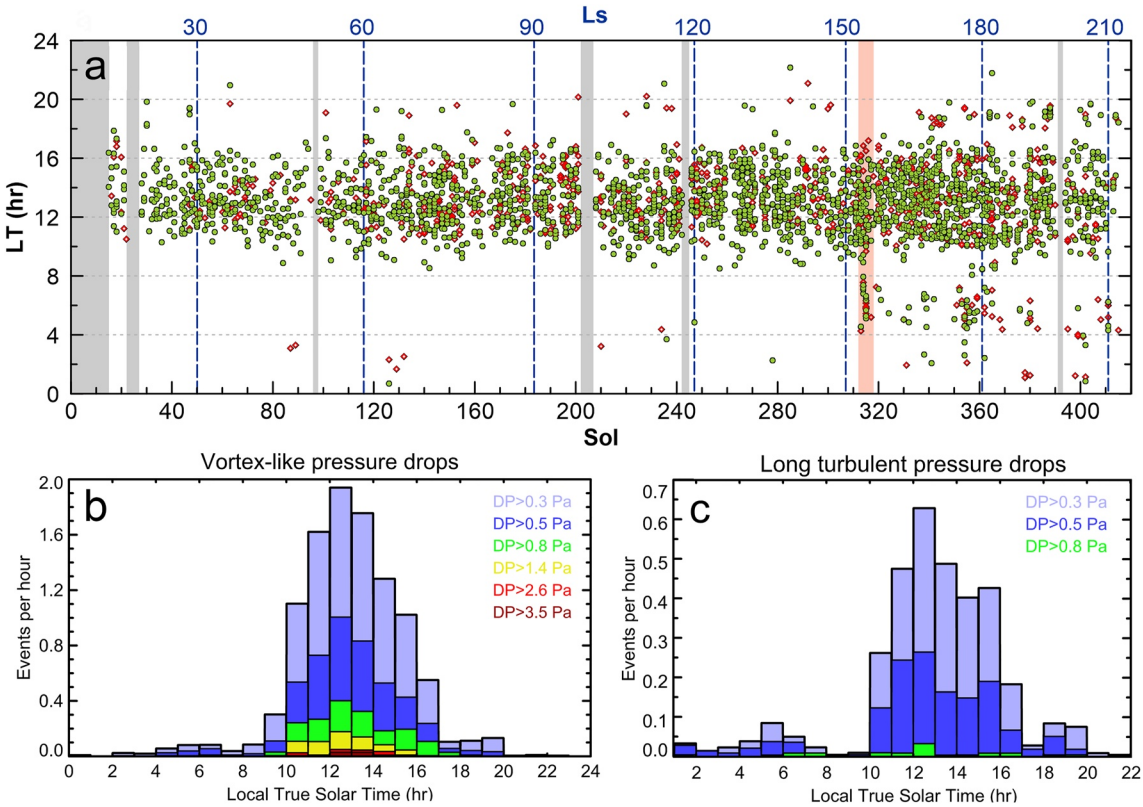

Figure 4. Distribution of pressure drops up to sol 415. (a) Distribution as a function of sol and *Ls*. Green circles show vortex-like pressure drops with $\Delta p > 0.3$ Pa identified from the shape of the pressure curve. Red diamonds show long pressure drops with pressure fluctuations indicative of turbulent events. The light orange dashed region highlights a period of time with an active dust storm over Jezero. Gray dashed regions indicate sols without data. (b) Daily distribution of pressure drops corrected from sampling effects. (c) Daily distribution of long pressure drops with turbulent fluctuations. The total number of vortex-like events in this plot is 2,283, and the total number of long and turbulent pressure drops is 759.

cells, as a remarkable event found on sol 117 and discussed in (Newman et al., 2022). However, the interpretation of the individual nature of these events requires examining additional data beyond pressure. In addition, pressure drops caused by atmospheric waves are also identified in the general pattern of pressure drops and eliminated from our study.

Figure 4 shows the temporal distribution of pressure drops, which are compatible with vortices with a pressure drop detection threshold of 0.3 Pa. These events are concentrated in the daytime hours with a peak activity near noon and tails of activity during the night. Long and turbulent events follow a similar daily distribution, and there is a fuzzy transition between both types of categories in events like those seen in Figure 3j.

There are clear changes in the overall activity of pressure drops over the time period of this study. An interesting change occurred on sols ~312–318 (Ls = 153°–156°), when a regional dust storm arrived and was active over Jezero enhancing DD activity (Lemmon et al., 2022). During the dust storm, increased pressure fluctuations were also observed, as well as a wealth of nighttime pressure oscillations (Sánchez-Lavega et al., 2022). However, this enhanced turbulence and increased vortex activity was significantly smaller than the burst of vortices and turbulence found by InSight during the dusty season at around Ls = 250° on MY35 (Aug. 2020) reported by Chatain et al. (2021). Future analyses over a full MY will be needed to assess if this change in activity in Jezero was caused by the dust storm, the local characteristics of the terrain, or seasonal evolution.

3.2. Vortices and Dust Devils

We identify DDs as events with a pressure drop of at least 0.3 Pa and a simultaneous reduction in irradiance captured by the RDS Top 7 sensor of at least 0.5% (corresponding to a $\Delta\tau = 0.05$). Figure 5 shows the temporal distribution of vortices (a; 2,283 events, where 1,056 events have a $\Delta p > 0.5$ Pa) and DDs (b-c; 238 events with

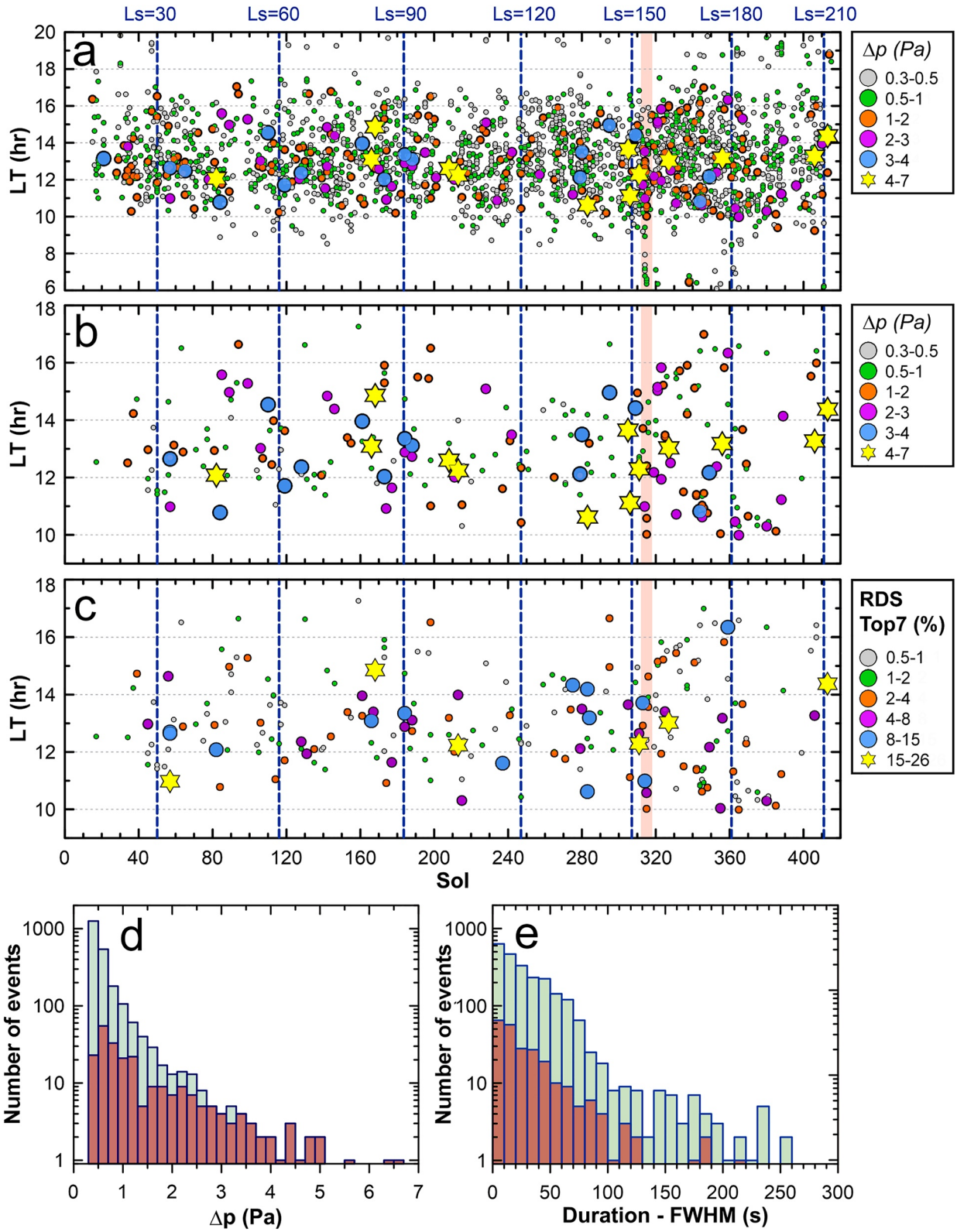

Figure 5. Distribution of vortices and dust devils (DDs). (a) Temporal distribution of vortices. Symbols identify events of different intensities. Panel (b) same as panel (a), but only for events with a Radiation and Dust Sensor (RDS) Top 7 detection of a dip in irradiance of at least 0.5%. Panel (c) same as panel (b) but showing here the level of dustiness of individual DDs. (d) Histogram of the number of events with a given pressure drop. (e) Histogram of the number of events with a given duration. Light green bars in panels (d and e) correspond to all vortices and dark brown bars correspond to DDs. The period of the dust storm is highlighted with a shaded region in panels (a–c). The total number of vortices with $\Delta p > 0.3$ and >0.5 Pa is 2,283 and 1,056, respectively. The total number of DDs in this sample is 238.

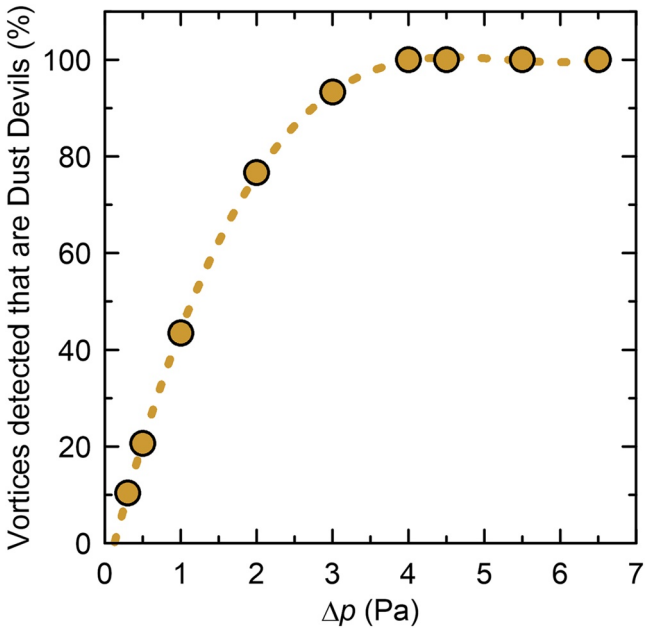

Figure 6. Percentage of vortices that are dusty with aRadiation and Dust Sensor Top 7 drop of at least 0.5% for pressure drops larger than the Δp values shown on the horizontal axis.

ΔRDS Top 7 > 0.5%). Panel (d) shows that intense vortices with large pressure drops tend to be dusty. This result is further explored in Figure 6. Only 1.8% of the vortices with a pressure dip from 0.3 to 0.5 Pa had a simultaneous detection of dust. About 20% of all pressure drops with $\Delta p > 0.5$ Pa have dust and this fraction increases for higher values of the pressure drop becoming 75% for events with $\Delta p > 2.0$ Pa and 100% for events with $\Delta p > 3.3$ Pa.

Figure 5e shows that the duration of vortices containing dust tends to be smaller than non-dusty vortices implying smaller diameters for DDs events. However, a few extremely long DDs with FWHM of up to 220 s are also found. Figure S3 in Supporting Information S1 details the distributions of FWHM of the population of vortices and DDs. Figure S4 in Supporting Information S1 shows examples of the six longest pressure drops containing dust, with readings of the RDS Top 7 detector peaking with variations of 0.5%–1.5% and centered at the time of the minimum pressure. These infrequent events do not have an important effect in the statistics presented in this work and they probably represent a transition from the long duration DDs observed at Jezero to the passage of the edges of convective cells rising small levels of dust. Some of them could be created by DDs embedded within larger wind gusts. None of the events in this sample is comparable to the large wind gust detected on sol 117 described by Newman et al. (2022).

The relationship between the intensity of the pressure drop detected, its duration, and observed dustiness is fuzzy and is explored in Figure 7. These aspects depend on a combination of distance to closest approach, vortex diameter, dust density in the DD, and solar illumination. Events with pressure drops higher than 2.0 Pa are typically short (<FWHM> = 26 s, with maximum FWHM of 160 s) and dusty. They probably represent relatively close encounters with DDs. Dusty events with detected pressure drops smaller than 1.0 Pa are more numerous and tend to be longer (<FWHM> = 41 s and maximum FWHM of 215 s). Those weak dusty pressure drops with long durations (FWHM > 40 s) might represent more distant DDs, whereas those with $\Delta p < 1.0$ Pa and FWHM > 40 s may represent weaker DDs/vortices. The very few DDs with pressure drops smaller than 0.5 Pa have <FWHM> = 20 s and might be DDs in the process of losing strength and vanishing, rather than detections of distant vortices carrying dust. Panel c in this figure also shows the distribution of DDs per hour corrected for the uneven temporal sampling with MEDA and can be directly compared with Figure 4b for the vortex activity.

4. Variability of Vortex and Dust Devil Activity

Perseverance moved about 10 km as the seasons evolved from early Spring to Autumn over the first 415 sols of the mission. Several changes in the vortex and DD activity were observed in this period. Although the number of pressure drops increases for smaller amplitudes in Δp, since events with pressure drops smaller than 0.5 Pa are more difficult to characterize and only represent a tiny fraction of the DDs detected, we restrict our exploration of seasonal variability for events with $\Delta p > 0.5$ Pa.

4.1. Seasonal Evolution

Figure 8 displays histograms of the daily activity of vortices corrected from sampling effects in four different periods. The data shows an increase of vortex and DD activity from the first observations on $Ls = 13°$ to the last ones analyzed at $Ls = 213°$, with a small decay of activity at around $Ls = 120°$.

Numerical models predicted that the most intense daily activity of vortices and DDs should occur at noon in early Summer around $Ls = 120°$ (i.e., sol 248) (Newman et al., 2021). The small decrease of activity found around $Ls = 120°$ in Figure 8 is an unexpected result. We have examined the evolution of the intensity of daytime winds at Jezero (which were comparable during the first three periods of time with values of 4.1 ± 0.4 ms^{-1} and cannot be examined after the WS failure in sol 313), atmospheric opacity (which slightly decreased at around $Ls = 120°$), variations of the Thermal Inertia and albedo of the terrain, and surface and air temperatures. We were unable to

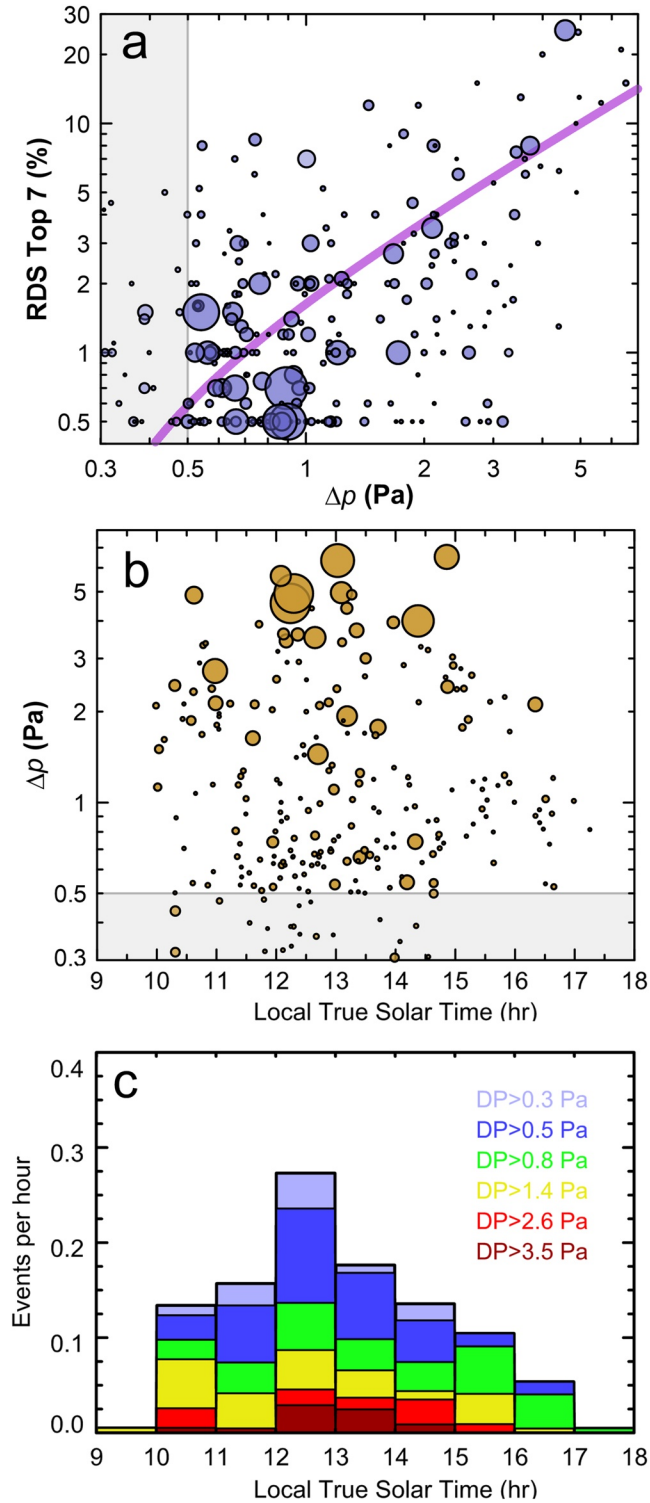

Figure 7. Dust devils (DDs) pressure intensity, duration, and dustiness. (a) Radiation and Dust Sensor (RDS) Top 7 decrease as a function of Δp. The circle diameter identifies the duration of each event from 1.0 (smallest) to 200.0 s (largest). The purple line is a fit to the data with a squared coefficient of regression $r^2 = 0.40$ (40% of the variations of the irradiance decrease is directly related to the variations in Δp). (b) Daily distribution of DDs. The circle diameter codifies the reduction of irradiance detected from 0.5% ($\Delta\tau = 0.05$) to 26% ($\Delta\tau = 0.30$). (c) Histogram of the number of DDs events per hour corrected from sampling effects associated to different sampling at different hours. All panels are based in the 238 dusty vortices found in Mars Environmental Dynamics Analyzer data, but the characteristics of the data make the survey incomplete for events from 0.3 to 0.5 Pa.

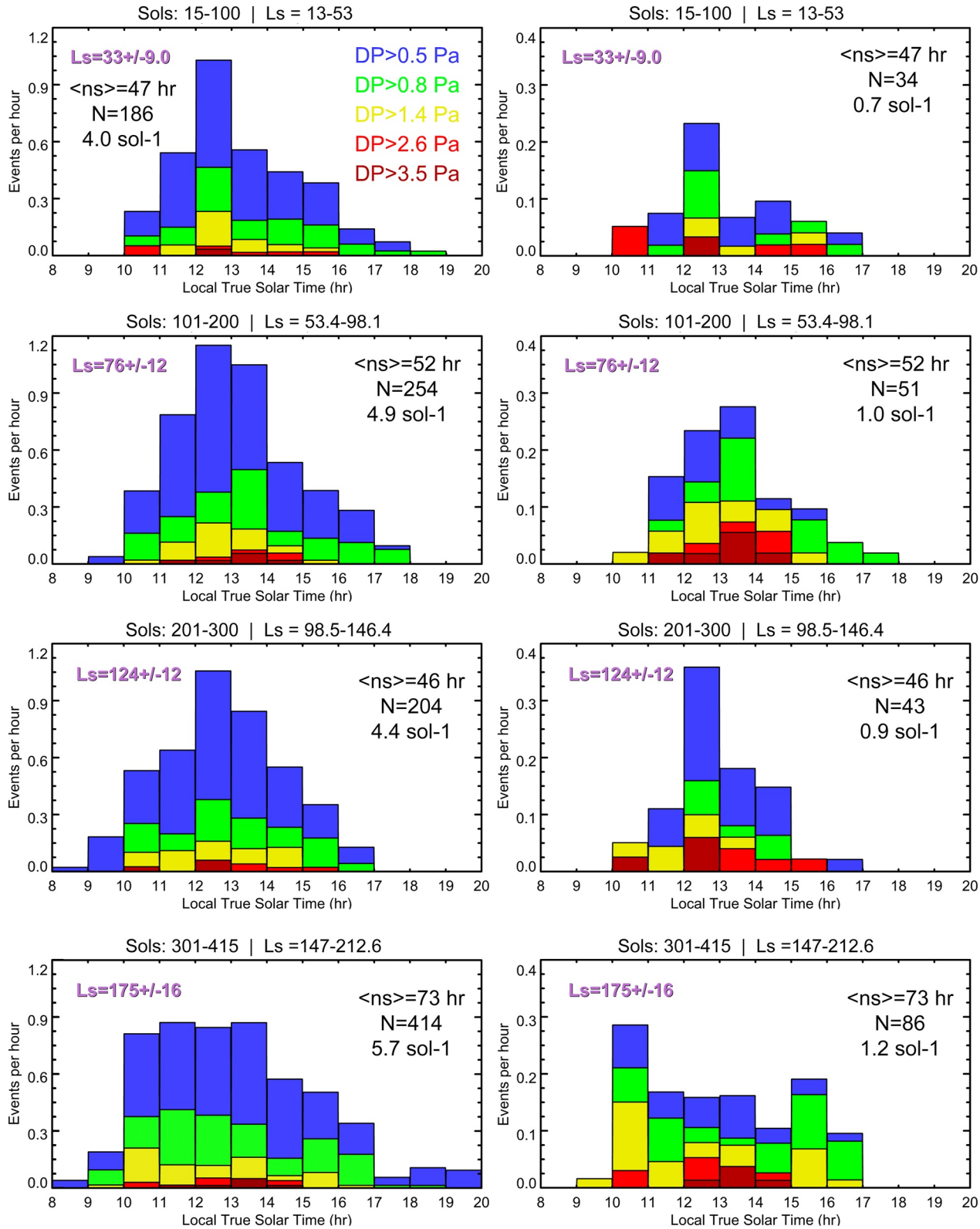

Figure 8. Daily histograms of vortices (left column) and dust devils (right column) over different periods. All histograms are corrected from sampling effects and observational gaps. The figure also shows the average number of hours observed each Local True Solar Time, n_s, the total number of events detected, N, and the mean number of events produced per sol in each period.

identify a specific variation that could explain this decrease of activity at $Ls = 120°$. A complex combination of small variations in these variables, combined with the stochastic nature of vortices encounters may explain this result, and data over different seasons will be needed to better understand the drivers of convective vortex activity at Jezero.

Maximum irradiation at noon at the top of the atmosphere occurred at the latitude of Jezero on sol 337 ($Ls = 166°$). This was a period characterized by higher atmospheric opacity and weaker surface-to-air temperature gradient than earlier in the mission. The maximum surface temperature at Jezero, and maximum near surface thermal gradient, was found around sol 280 ($Ls = 136°$) (Munguira et al., 2023), which is close to the cluster of strong DDs found on sols 304–328, including the period covered by the dust storm. This result is in agreement with the correlation found by Spiga et al. (2021) between the increased number of diurnal vortices and the higher surface temperatures found by InSight.

4.2. Dust Devil Activity During the $Ls = 153°$ Dust Storm

A regional dust storm passed over Jezero from sols 312 to 318 ($Ls = 153°$–$156°$). The storm brought significant changes in atmospheric opacity (Lemmon et al., 2022), temperatures (Munguira et al., 2023), and behavior of pressure (Sánchez-Lavega et al., 2022), and also mobilized large amounts of dust and sand that caused a decrease in surface albedo. Lemmon et al. (2022) present a detailed study of the dust storm. DD Surveys and DD Movies obtained by Perseverance's cameras during the dust storm resulted in a record number of 14 DDs imaged on sol 313 over 11:35–11:59. MEDA recorded eight vortices with $\Delta p > 0.5$ Pa over 10:12–14:10 on that sol, and one of these vortices damaged one of the MEDA WSs (see Section 7).

MEDA detections of vortices and DDs around and during the dust storm period are presented in Figure 9. Most of the vortices detected over sols 313–315 were weak in terms of their Δp, and part of the enhanced activity seems to be associated to weak and short pressure dips that appear anomalously early over the sol at LTST of 04–08 hr. These sols exhibited a higher dust opacity that reached its peak of $\tau = 2.4$ on sol 314. They were accompanied by a decreased near-surface thermal gradient relative to previous sols, which was caused by increased air temperatures with near noon values of +14 K without significant changes in surface temperatures compared with previous sols (Munguira et al., 2023). Pressure oscillations not related to vortex activity started to be numerous around sol 313 and changed the pattern of small nighttime pressure oscillations after the dust storm died away (Sánchez-Lavega et al., 2022). Although the sampling cadence over this period was higher than in previous sols (Figure S1 in Supporting Information S1), the increase in DD detections is significant. DDs in Figures 9b and 9c show a concentration of 1.5 events detected per sol that translates in 2.0 events per sol once corrected for the time sampling over sols 310–318, doubling the inferred activity for that seasonal period. There were no DD events and very few vortices detected on the last two sols of the storm (317–318), which also corresponded to lower surface and air temperatures and reduced surface-to-air thermal gradient (Munguira et al., 2023). The recovery to normal environmental conditions occurred in sol 318, when the dust opacity (Lemmon et al., 2022), pressure (Sánchez-Lavega et al., 2022), and temperatures (Munguira et al., 2023) returned to normal levels.

The DD activity during the dust storm was very different to that observed by Curiosity at Gale crater during the MY34/2018 Global Dust Storm (Guzewich et al., 2019), when a strong suppression of vortex activity was observed for most of the storm (Ordóñez-Etxeberria et al., 2020). This suppressed vortex activity occurred when the dust opacity grew to $\tau = 3.5$, and vortex activity recovered when the dust opacity diminished to $\tau = 1.5$. The situation at Jezero was more similar to that observed by InSight during a Large Dust Storm (LDS) on 2019 (Viúdez-Moreiras et al., 2020). The MY34/2019 LDS developed at $Ls = 320°$, reaching peak values of $\tau = 1.9$ with a duration of ∼110 sols. InSight observed an enhancement of vortex activity during the storm onset, and a reduction in its long decaying phase. In the 2022 dust storm at Jezero, there was a cluster of intense events before the storm, an increase of activity over sols 313–315 with a dust opacity peak of $\tau = 2.4$ on sol 314, and a reduction of activity over the decaying phase of the dust storm that extended only until sol 318, when τ was down to 1.3 (Lemmon et al., 2022). This phenomenology represents a faster version of what was observed by InSight during the longer-lived 2019 LDS.

4.3. DD Activity, Terrain Properties, and Vertical Thermal Gradient

There are fundamental differences between meteorological stations fixed in a landing site (Viking Landers, Phoenix and InSight) and those in moving rovers (Mars Exploration Rovers, Curiosity, Zhurong, and Perseverance) that sample atmospheric properties over different terrains. Martínez et al. (2021) investigated the possible relations

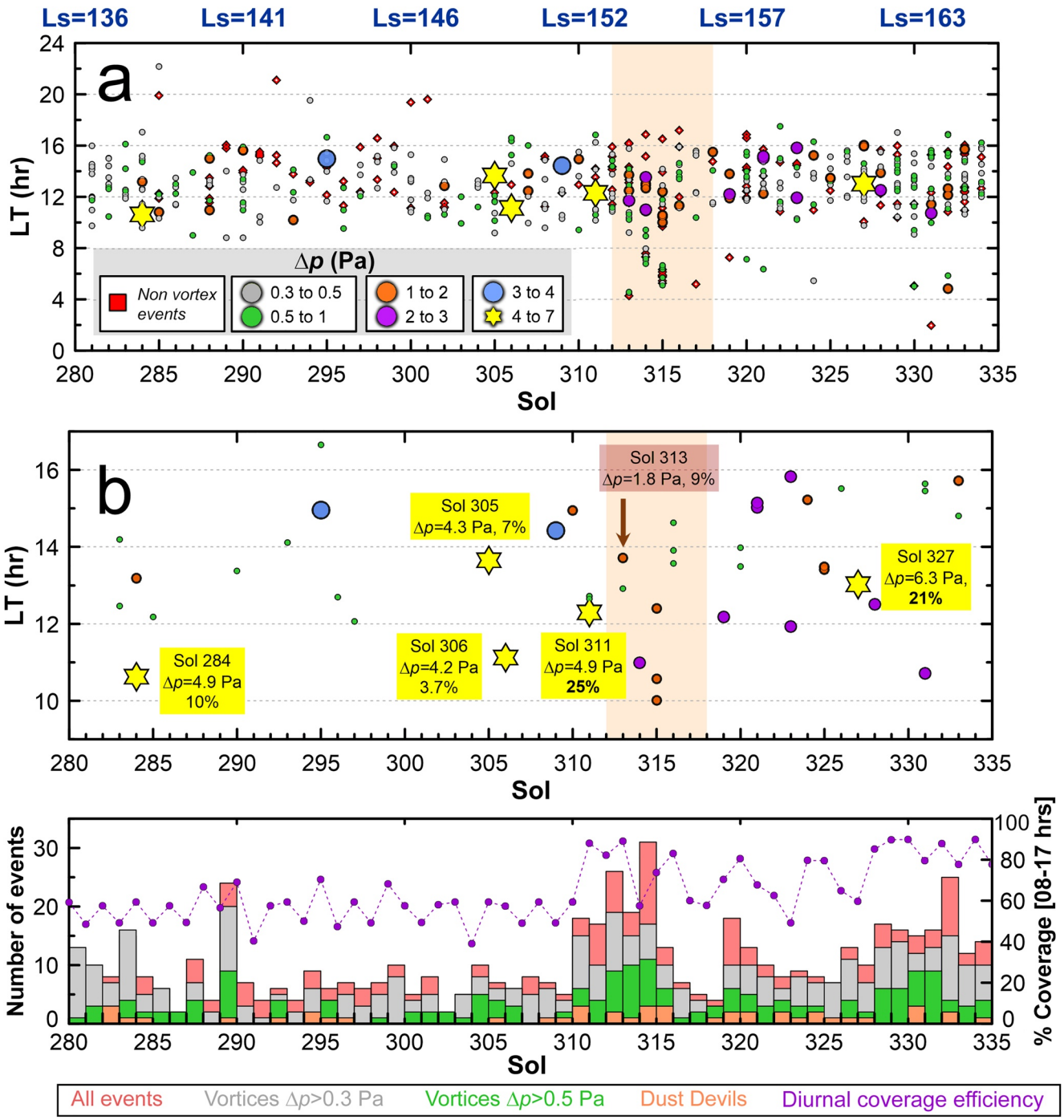

Figure 9. Vortex and dust devil (DD) activity during the dust storm. (a) All pressure drops from sols 280 to 335. (b) DDs in the same period. Red squares in (a) correspond to pressure drops not caused by vortices. Symbols identify the intensity of the pressure drop. Shaded areas highlight the period of dust storm over Jezero. The intensity Δp of individual events and percentages of the reduction of light measured by Radiation and Dust Sensor are given in panel (b) for selected events. A DD highlighted with an arrow in panel (b) damaged part of the hardware of one wind sensor on sol 313 at 13:38 Local True Solar Time (LTST). (c) Number of vortices DDs detected per sol compared with the diurnal coverage of Mars Environmental Dynamics Analyzer data from 08 to 17 LTST.

between the Thermal Inertia (TI) of the terrain, the vertical thermal gradient of the atmosphere, and vortex activity at Gale crater from data obtained with the Curiosity rover for 2500 sols. They concluded that the strong inter-annual variability of vortex activity found at Gale crater by Ordóñez-Etxeberria et al. (2020) was mainly a consequence of the rover ascent over Aeolis Mons and was not only caused by variations in properties such as

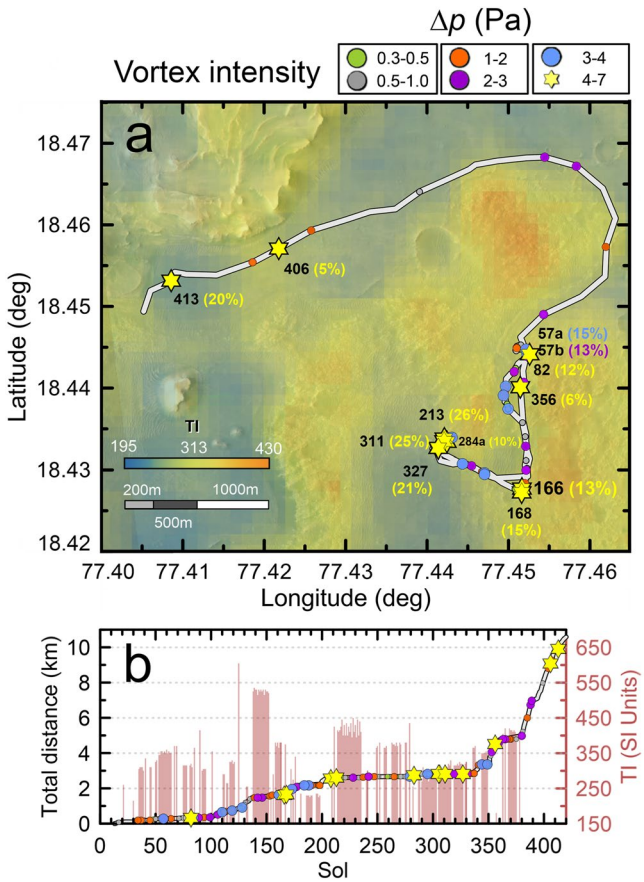

Figure 10. Dust devils (DDs) over Perseverance's traverse. (a) THEMIS map of thermal inertia, rover traverse (line) and DDs identified with symbols quantifying the intensity, Δp of the pressure drop. Black numbers correspond to sols with the most intense events. Colored numbers give the percentage of light decrease in Radiation and Dust Sensor Top 7. (b) Distance traveled by Perseverance (gray line, left axis) compared with thermal inertia of the terrain derived from Mars Environmental Dynamics Analyzer data (vertical bars, right axis) with individual events superimposed following the same symbols as in panel (a).

the thermal inertia of the local terrain. Spiga et al. (2021) investigated the seasonal variations of vortex activity at Elysium from InSight data, finding a clear correlation between the number of vortices and high values of surface temperatures with a weaker correlation with values of the vertical thermal gradient. We examine MEDA data, where we have a more homogenous data set that Curiosity, without strong variations in the topography of the terrain traversed, and with different surface properties unlike the measurements by InSight at a single location.

MEDA has found out strong variations of the TI of the terrain at spatial scales smaller than those sampled from orbit. TI with MEDA is measured from a combination of TIRS and RDS data (Martínez et al., 2023; Rodriguez-Manfredi et al., 2023) resulting in values of TI that range from 180 to 610 $Jm^{-2}K^{-1}s^{-1/2}$ (TI units hereafter). These values are comparable to those obtained from orbit by the THEMIS instrument (Fergason et al., 2006) on the Mars Odyssey orbiter. THEMIS data in the Jezero region has a spatial resolution of ~100 m × 100 m, and average values of Thermal Inertia of ~300 TI units. MEDA measures values of TI over small patches of the terrain observed in the FOV of TIRS, which covers an area of 3 m^2, which is a significantly smaller area than the 100 m^2 used by Curiosity at Gale (Gómez-Elvira et al., 2012). However, the range of TI variations at Gale crater from Curiosity measurements (Martínez et al., 2021) is comparable to those found at Jezero by Perseverance.

MEDA measurements in Jezero show that variations in the values of TI over the rover's traverse correlate with strong variations in the vertical thermal gradient of the atmospheric surface layer (Munguira et al., 2023; Rodriguez-Manfredi et al., 2023). This is the expected behavior in Mars, because terrains with low values of TI favor higher near-noon surface temperatures and higher vertical thermal gradients, which is a key element in producing convective vortices (Rennó et al., 1998). In addition, the TI of the terrain can be modified by its dust cover, with more dusty terrains resulting in lower values of thermal inertia than rocky terrains without a dust cover (Martínez et al., 2023; Putzig & Mellon, 2007). Figure 10 shows a map of Jezero's TI from THEMIS data with the rover's trajectory and the DDs detected. We show the intensity of the pressure drop of individual events and the decrease of light measured by RDS on the dustiest DDs. These are compared with the derived values of thermal inertia from MEDA up to sol 380 (later sols correspond to frequent drives during a rapid traverse phase that did not allow to measure TI). Figure 10b shows that intense DDs over terrains with high TI are uncommon.

Figure 11 shows relations between vortex properties, the vertical thermal gradient of the atmosphere from the difference between the surface temperature and the air temperature at 40 m, and the TI of the terrain. The vertical thermal gradient is calculated for a time window of 8 min around the vortex passage, and is a function of LTST and surface TI with only minor effects from seasonal changes. The daily distribution of vortices as a function of the vertical thermal gradient shows that local terrains with values of thermal inertia larger than 400 TI rarely produce vertical thermal gradients at noon larger than 25 K, and the associated vortices are less intense and have a lower probability to become DDs. We note that the distribution of DDs follows the same trend as that of the intense vortices. Figure S5 in Supporting Information S1 shows a scatter plot of pressure drops of DDs and the vertical thermal gradient during these events also showing their observed dustiness from the RDS Top 7 decrease of irradiance. The most intense events do not always correspond with the strongest vertical thermal gradients, but those with $\Delta P > \sim 3$ Pa coincide with a surface-to-atmosphere difference of at least 20 K.

The correlation of vortices with a vertical gradient of temperature is equivalent to the correlation with the surface temperatures (Figure S6 in Supporting Information S1), and differences with results reported by Spiga

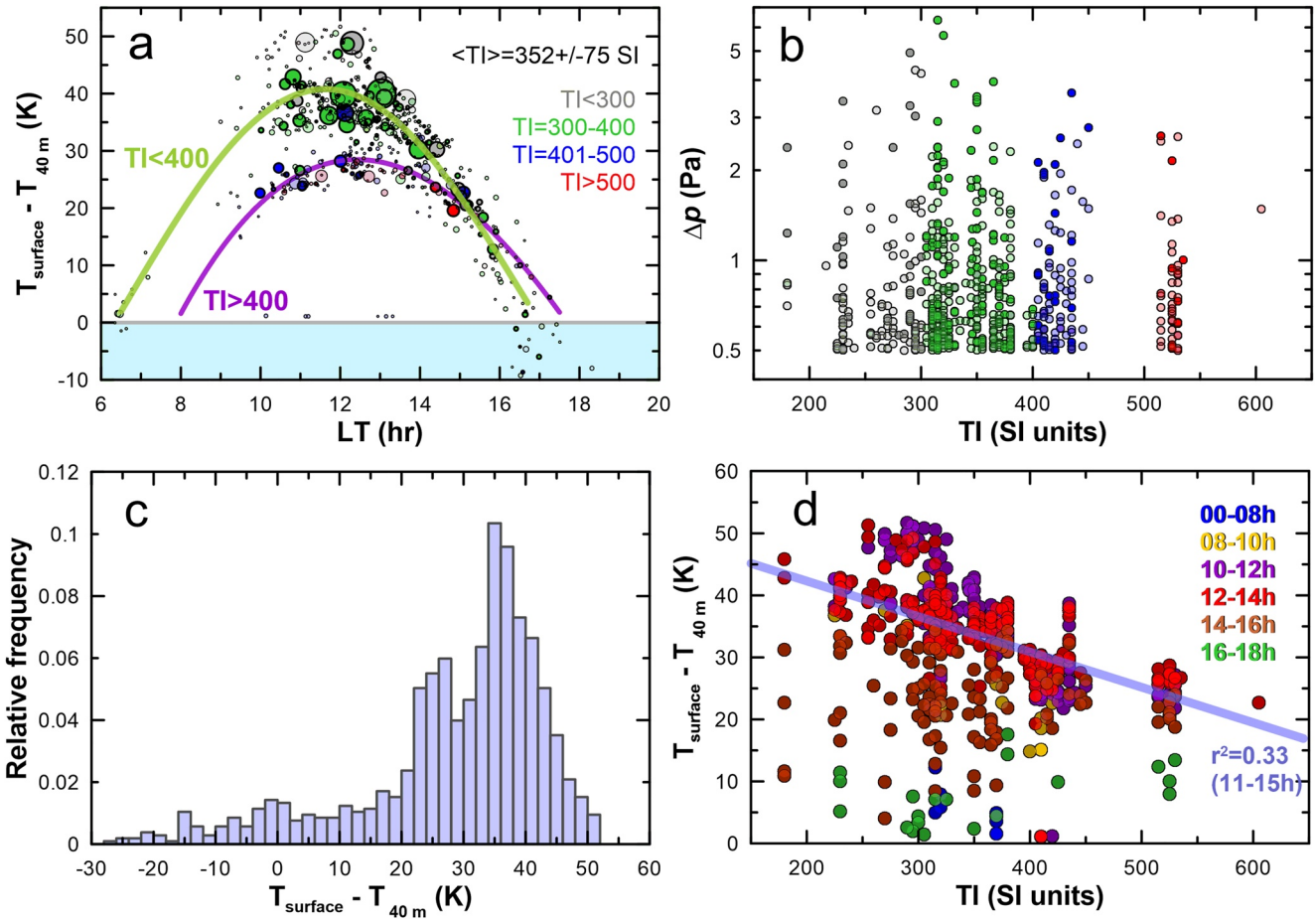

Figure 11. Vortices intensities in terms of their Δp, vertical thermal gradient of the atmosphere, and surface thermal inertia. (a) Distribution of vortices as a function of Local True Solar Time and the vertical thermal gradient. Individual vortices are plotted with circles whose diameter indicates the intensity of Δp from 0.5 (smallest) to 6.5 Pa (largest). Colors correspond to different values of the surface Thermal Inertia (TI). Vortices are shown with light shaded colors and circles with thin lines, while DDs are shown with dark colors and circles with thicker lines. Polynomial fits to vortices found over terrains with TI < 400 and >400 are shown with green and red lines respectively. The r^2 coefficient of determination of the fits are 0.84 and 0.62 in the green and purple lines respectively. (b) Scatter plot of the intensity of pressure drops for all vortices compared with the values of the local TI. Colors correspond to those used in panel (a) indicating non-dusty vortices (light colors) and DDs (dark colors). (c) Histogram of the number of vortices found for different values of the vertical thermal gradient. (d) Relation between the surface TI and the vertical thermal gradient during vortex detections. Circles identify different vortices and colors their Local True Solar Time. A linear fit to data close to noon hours is shown with a blue line.

et al. (2021) for InSight are likely a consequence of the lower capability of InSight to determine the vertical gradient of temperature, which is possibly due to the location of the InSight air temperature sensors facing out over the solar panels.

Field data and models of vortex formation (e.g., Rafkin et al., 2016) show that convective vortices are embedded within larger convective structures with spatial scales that are much larger than the surface variations of TI characterized with MEDA. This is a major factor that contributes to the scatter of vortex properties shown in Figure 11. However, the correspondence between TI and strong pressure drops indicates that, at least to some degree, surface variations are affecting vortex intensities at relatively small spatial scales as the vortices move over a terrain with inhomogenous temperatures.

5. Physical Properties of Dust Devils From Model Fitting

Our vortex and DD observations are sensitive to a combination of the physical properties of the vortex and the geometry of its encounter with the rover. In order to obtain realistic values of the physical parameters of DDs we compare pressure and wind data of MEDA vortices with a model of a drifting vortex (R. D. Lorenz, 2016) following a similar approach to Kahanpää and Viúdez-Moreiras (2021) without fitting the RDS signals. We calculate

Table 1
Parameters Defining a Vortex Encounter

Vortex parameters	
Δp_0	Pressure drop at the vortex center
D	Diameter of the vortex (maximum winds)
S	Vorticity sign: Positive for counter-clockwise rotation, negative for clockwise
α	Cyclostrophic factor from 0.5 (fully cyclostrophic) to 1.0
Geometrical and environment parameters	
$d_{\min}$	Minimum distance
Path	(+) for vortices at y positive when closest
	(−) for vortices at y negative when closest
U	Vortex drift velocity
Ω	Vortex drift direction angle (measured clockwise from the North)

the pressure drop at the center of the vortex, ΔP_0, and its diameter D, together with the trajectory of the vortex and its minimum distance to Perseverance.

5.1. Methodology

We assume vortices that move in a straight line with the environment winds. The parameters that define the pressure and winds created by the combination of a moving vortex and the environment winds observed at a fixed location are given in Table 1. We also assume a Lorentzian pressure drop and vortices close to cyclostrophic equilibrium that follow:

$$V_t = \sqrt{\alpha \Delta p_0 / \rho}, \quad (1)$$

where, V_t is the maximum tangential velocity of the vortex at the vortex edge, Δp_0 is the pressure drop at the vortex center with respect to the environment, ρ is the atmospheric density, and α is a free parameter from 0.5 to 1.0 that allows deviations from cyclostrophic, with 0.5 representing a fully cyclostrophic vortex (see discussion in Kurgansky et al., 2016).

We implement the numerical model from R. D. Lorenz (2016) and follow a Monte-Carlo approach to find the combined set of parameters that best fit MEDA pressure and wind data for individual vortex encounters. For each vortex we generate random values of all the parameters in Table 1 within reasonable ranges for each parameter, and compare the modeled pressure and winds with MEDA observations. Because we are sampling a six-dimensional space of parameters (plus the uncertainty in vortex rotation and path) we test ~20,000 – 50,000 models for each of the MEDA vortices analyzed. We calculate values of χ^2 for pressure and wind and we use a combined figure of merit χ^2 to select the best fits. The parameters of models that best approach the observations of a MEDA vortex converge in narrow ranges. To refine the fits, we launch a second set of 20,000–50,000 models in the parameter region that contains the best models. The parameters that best reproduce the observations are defined with the statistics of the 10 best models, which are visually examined to confirm they represent a close match to the observations. Figure S7 in Supporting Information S1 shows an example of the procedure for the strong DD observed on sol 82 (see Figure 2). Cases in which a visual match of MEDA data and model results is not found also result in unconstrained model parameters with large range of possible values. These cases are eliminated from the analysis presented. In practice, this means that complex vortices with pressure curves with inner structures, those with noisy wind measurements, and those with weak pressure drops cannot be fit efficiently.

For the DD on sol 82 shown in Figure 2 with $\Delta p = 5.6$ Pa and an RDS Top 7 drop of 12%, Figure 12 shows a comparison of the three best models and the MEDA data. The parameters that fit the DD on sol 82 correspond to a vortex with a diameter of 11.4 ± 4.0 m passing at a closest approach of MEDA of 0.0–0.4 m with a mean crossing distance of 0.15 m and anticlockwise rotation. Such a close approach implies a central pressure drop of 5.6 ± 0.3 Pa essentially identical to the one observed by MEDA. Because of the stronger variations in winds

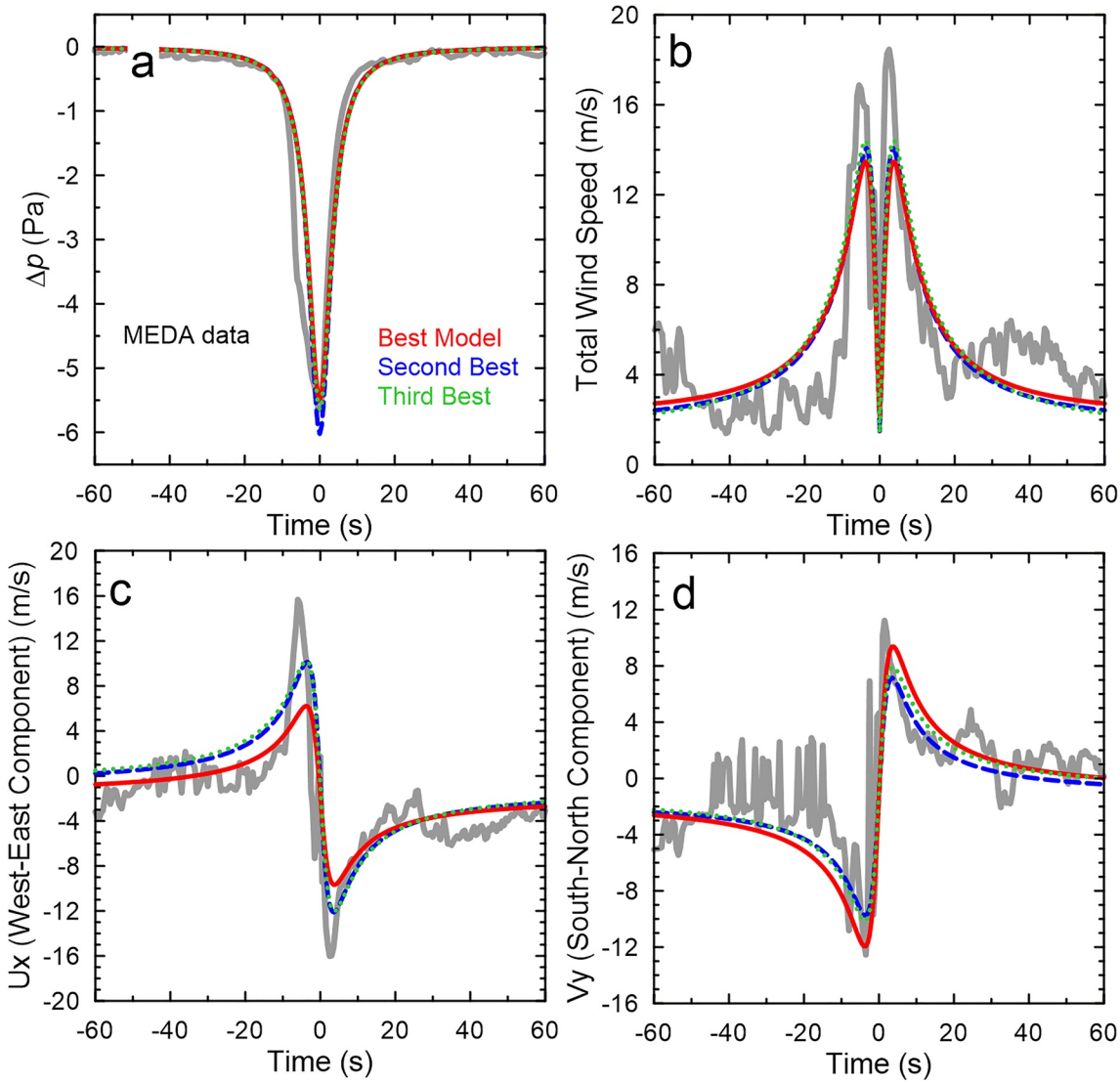

Figure 12. Comparison of Mars Environmental Dynamics Analyzer (MEDA) data and best models for the dust devil on sol 82. (a) Pressure. (b) Total wind speed. (c) Zonal (west to east) component of the wind. (d) Meridional (south to north) component of the wind. Gray lines show MEDA data. Colored lines show the best three models.

than in pressure, crossing distances are more representative of the distance to the rover WSs than to the pressure sensor.

This method has been validated for a DD on sol 215 also imaged by Navcam and observed acoustically by the SuperCam Microphone (Murdoch et al., 2022). Vortex properties were obtained independently from Monte-Carlo modeling of the MEDA data, from the acoustic data, and from images, and were found to be highly consistent with each other.

5.2. Results

There are 131 DDs with wind data in the MEDA data presented here. We selected 22 events that we analyzed individually. These DDs were selected because they were the most intense, more dusty, and those with a strongest wind signature. This implies a strong bias toward close encounters with DDs. An event specifically selected to explore this bias is the DD on sol 264, whose pressure curve is shown in Figure 3g, and has a wide central pressure drop that could be considered as representative of a distant vortex. This event was accompanied by a weak reduction of irradiance in the RDS Top 7 with longer signals in the RDS Lat detectors.

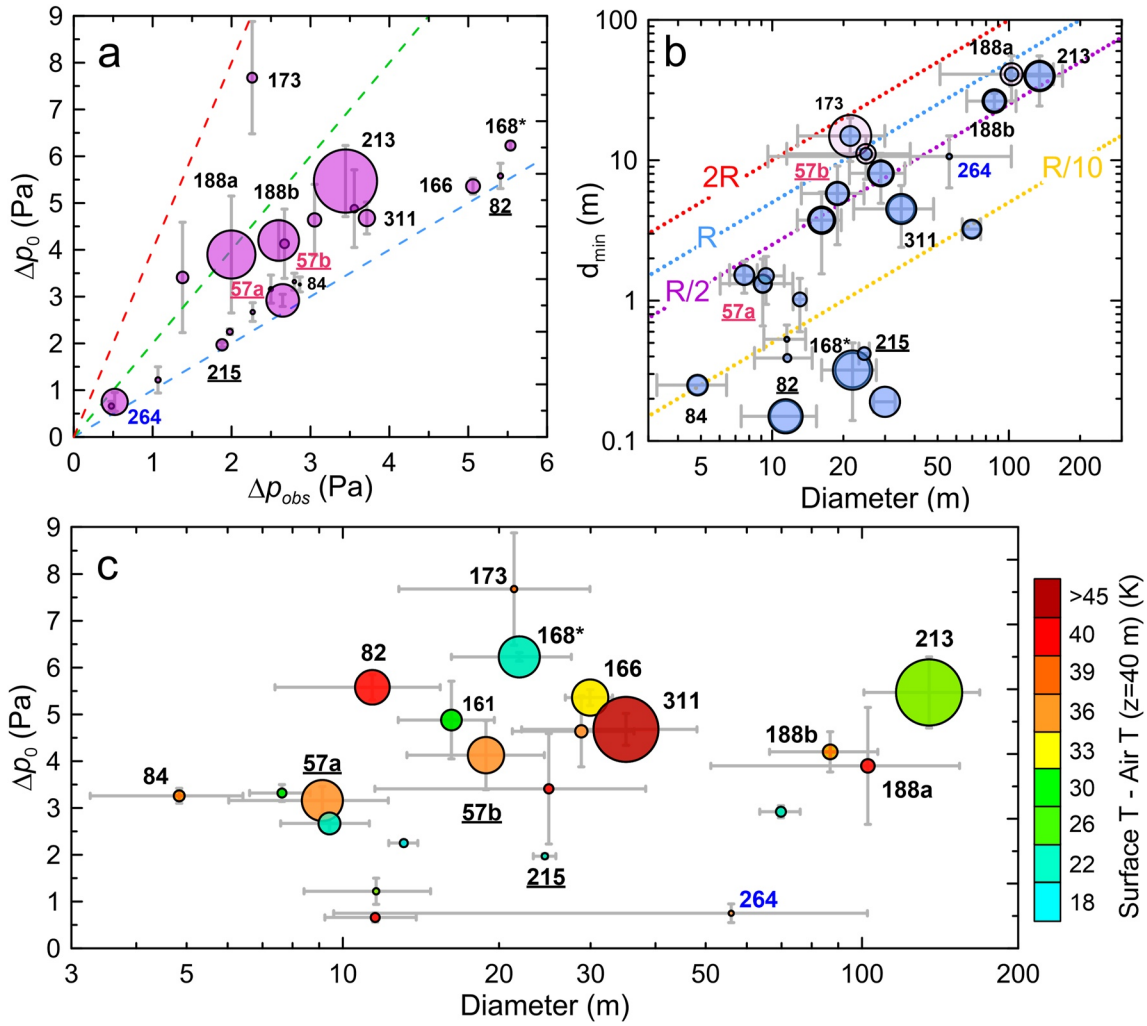

Figure 13. Dust devils from modeling pressure and winds. (a) Δp_0 at the vortex center as a function of the observed Δp_{obs}. Circle sizes represent vortex diameters from 4.8 to 135 m. Dashed lines correspond to $\Delta p_0 = n\Delta p_{obs}$ with n = 1, 2, 3 (blue, red, and green, respectively). (b) Minimum distances compared to vortex diameters. Circle sizes indicate the observed pressure drop (inner circle) and the vortex center (outer circles). Diagonal dotted lines show crossing distances as a function of the vortex radius R. (c) Scatter plot of vortex central pressure drop and vortex diameter. Circle sizes indicate irradiance decrease in the Radiation and Dust Sensor Top 7 from 0.5% to 26%. Numbers indicate sols of specific events. Underlined events have been specifically modeled here or in Murdoch et al. (2022). Colors indicate the thermal gradient of the atmospheric surface layer (T ground − T air at z ~40 m) for each event.

Our results for the sample of 22 vortices result in values of $\alpha = 0.65 \pm 0.08$ with 40% of the vortices having clockwise rotation and 60% having anti-clockwise rotation, which implies an equal distribution of the sense of rotation. Figure 13 shows the results for our fits to DDs. These DDs have central pressure drops comparable or up to twice the observed Δp in MEDA data. Most events have crossing distances smaller than the vortex radius, and only a few events are observed at a distance comparable to the vortex diameter. For the DD on sol 264 that was selected to test distant passages, we find that while our model simulations converge toward a close encounter, there are very large error bars associated with the small pressure perturbation and weak winds observed during this event.

The vortices have diameters from 4.8 to 135 m, the latter found in the event in sol 213 at 12:14 LTST. This DD was discussed by Newman et al. (2022), as it was a dusty event with a reduction in the RDS Top 7 irradiance of 26% ($\Delta\tau = 0.3$, the largest in 415 sols). This large opacity can be explained by a dusty vortex with a diameter of 135 m crossing at a minimum distance of 40 m from Perseverance. Paradoxically, this intense and large event occurred under a small vertical thermal gradient over a terrain with a relatively high local surface thermal inertia of 420 SI units. However, this was a large vortex that may have formed over nearby terrains with a more typical vertical thermal gradient.

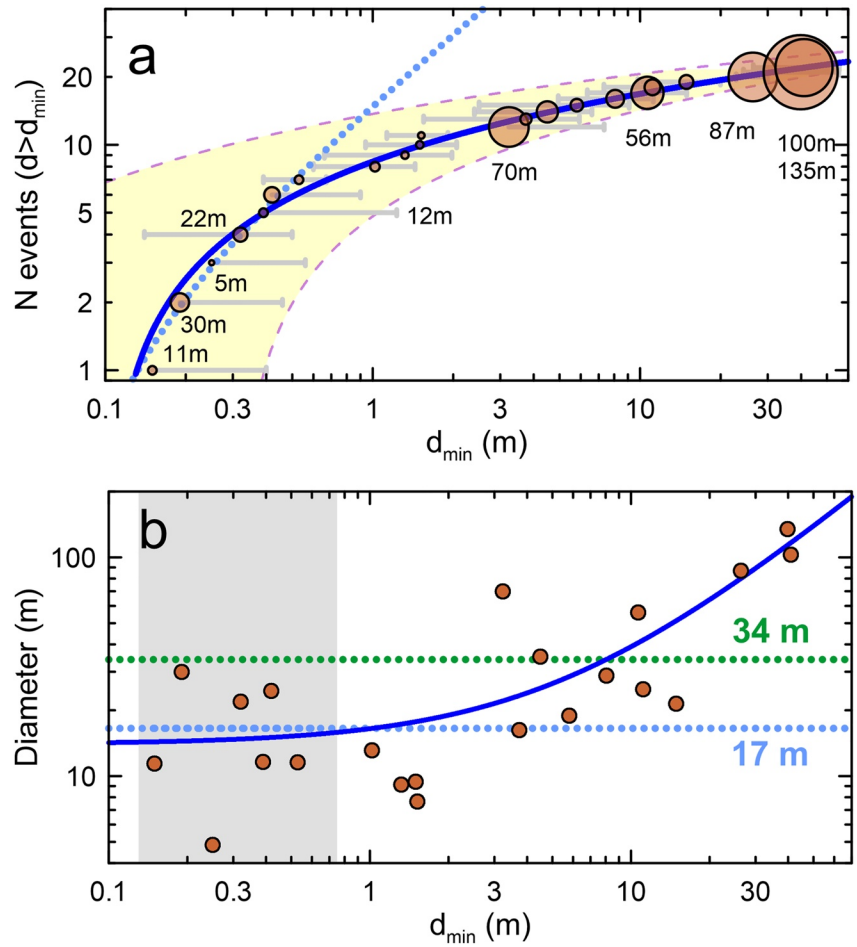

Figure 14. Crossing distances and diameters of dust devils (DDs). (a) Cumulative distribution of DDs as a function of their crossing distance. Circles represent individual events with the size of the circle representing vortex diameters from 5 to 135 m. Error bars are calculated from the Monte-Carlo fits to each event. The blue line is a logarithmic fit to all the data. The dotted line is a linear fit to the first seven events extended to the limits of the plot. (b) Diameter of individual DDs as a function of their crossing distance. Events with a crossing distance smaller than 1 m appear in the shadowed area. The blue solid line shows a linear fit to all the data. The light blue dotted line shows the average of the seven closest events suggesting that the most common diameter is 17 m. The green dotted line shows the average of all DDs that have a calculated diameter.

We note that the estimation of the size scale of this event given in Newman et al. (2022) was 300 m, estimated as the distance traversed during the FWHM of the event at the environment wind speed u. Here we find a smaller diameter of 135 m from our fits to models of this event. We interpret the distance obtained in Newman et al. (2022) as the distance traveled by the vortex while its properties can be sensed by MEDA. Given its minimum crossing distance (40 m) and size (68 m in radius), the vortex was detected at distances of 150 m, or 2.3 times its radius. For most of the vortices that we have modeled, we find that the estimated diameters given in Newman et al. (2022) should be corrected by dividing by 2.0. Newman et al. (2022) considered that DDs and infrequent wind gusts raising dusts over large areas contribute approximately equally to lifting dust in Jezero. Although we now estimate smaller diameters for DDs in Jezero, we have not found new wind gusts on MEDA data equivalent to the one reported by Newman et al. (2022), which makes dust lifting by both, infrequent large wind gusts, and regular DDs still comparable.

Another interesting DD is the event on sol 173 at 12:01 LTST. This was a 3.2 Pa pressure drop with a temporal duration of 45 s. The vortex was accompanied by variations in the winds of 20 ms^{-1} and a small reduction of irradiance at the RDS Top 7 sensor (0.5%, $\Delta\tau = 0.05$). The parameters that fit this event converge in a vortex with a diameter of 12–30 m crossing at a distance of 10–20 m. This intense vortex may have had a central pressure

drop of 6.5–9.0 Pa. This upper limit is similar to the most intense vortices directly detected at Elysium Planitia by InSight (Spiga et al., 2021).

From our model fits to the most intense vortices we have found their likely crossing distances. There are seven DDs for which the vortex center is modeled to have passed within 1 m of Perseverance. These vortices are sensed in their true magnitude and provide an unbiased sample of the properties of vortices at Jezero. Figure 14a shows the vortices whose properties we have been able to fit ordered with respect to their minimum crossing distance. A linear fit to the seven vortices with closest approaches has an r^2 regression coefficient of 0.986.

We examine the distribution of diameters in Figure 14b. For the very close approaches, representing an unbiased sample, the diameters of the vortices characterized is 17 ± 8 m, which is comparable to the diameters of vortices in images of Jezero shown in Newman et al. (2022). There are three vortices with a diameter of 100 m passing at a distance of 30 m and the mean diameter of all the vortices with model fits is 34 m. Thus, while the average diameter of vortices at Jezero can be constrained to 25 ± 8 m, most DDs at Jezero have diameters of ∼17 ± 8 m. In addition, the events with crossing distance below 1.0 m have central pressure drops from 0.7 to 5.6 Pa with an average value of 3.5 Pa. This can be considered as a typical central intensity of frequent vortices at Jezero. More intense events, with values of central pressures up to 9.0 Pa appear only rarely, and we have only observed one of them at a large distance resulting in a smaller value of observed Δp.

The distance of approach of the closest passing vortices and the frequency at which we observe the largest vortices constitute a set of strong constraints on the density of DDs in Jezero and their size distribution, as will be analyzed in Section 7.

6. Comparison With LES Results

In order to gain further insight in to the complexities of characterizing a sample of vortices from measurements obtained with a single station, we explore vortices in a LES representative of the conditions at Jezero and analyze the data from the simulation with the same algorithm used for MEDA. We examine one MarsWRF (Richardson et al., 2007) simulation of Jezero crater in LES mode (Newman et al., 2022; Wu et al., 2021). The LES grid has a horizontal resolution of 10 m over a region covering 10 × 10 km with periodic boundary conditions. The model output is given every 10 s. A background wind of 4 m/s, comparable to daytime winds at Jezero, is imposed. The latitude, surface properties (height and albedo), and TI of the surface are chosen to match those of Jezero crater, with a TI constant value of 270 SI representative of the region. Solar irradiation, dust loading and radiative effects were chosen to match those expected at Jezero at $Ls \sim 45°$. The simulation is started at 06:00 LTST and continued through 15:00 without obvious spin-up effects after the simulation reaches 10:00 LTST. Results presented below correspond to half an hour starting at noon.

6.1. Vortices and Pressure Drops in the LES

The LES shows the presence of intense vortices mixed with convective cells and turbulence. Figure 15a shows a snapshot of the simulation where vortices create local minima of pressure. Figure 15b shows the tracks of the 20 most intense vortices in each time step of the simulation as they drift over half an hour. In that period, vortices evolve in intensity and can vanish or merge with new vortices being produced in other locations. The strongest vortex was observed with a peak pressure drop of $\Delta p_0 = 8.0$ Pa, and there was always at least one vortex with $\Delta p_0 = 5.0$ Pa within the 100 km^2 domain.

6.2. MEDA and Model Comparison

We positioned 400 synthetic stations at regular distances covering the simulation domain and analyzed the pressure time-series at each station using the same vortex detection algorithm used for MEDA including the analysis of data from multiple time windows. The 400 stations operating over the period of the simulation examined are representative of 400 sols at noon with a total analysis time of 200 hr. This number is comparable to our analysis of MEDA data at noon for 415 sols, which accumulates 242 hr of observations for the 12:00–13:00 time range.

The most intense pressure drop found with the MEDA algorithm in the LES corresponded to an event with a pressure deficit of only $\Delta p = 2.7$ Pa with a FWHM of 25s (Figure 15c). The true characteristics of this vortex are shown in Figure 15d. The event is a vortex of 85 m in diameter crossing at a minimum distance of 20 m of the meteorological station with a $\Delta p_0 = 3.35$ Pa. There are many other more intense vortices in the simulations that

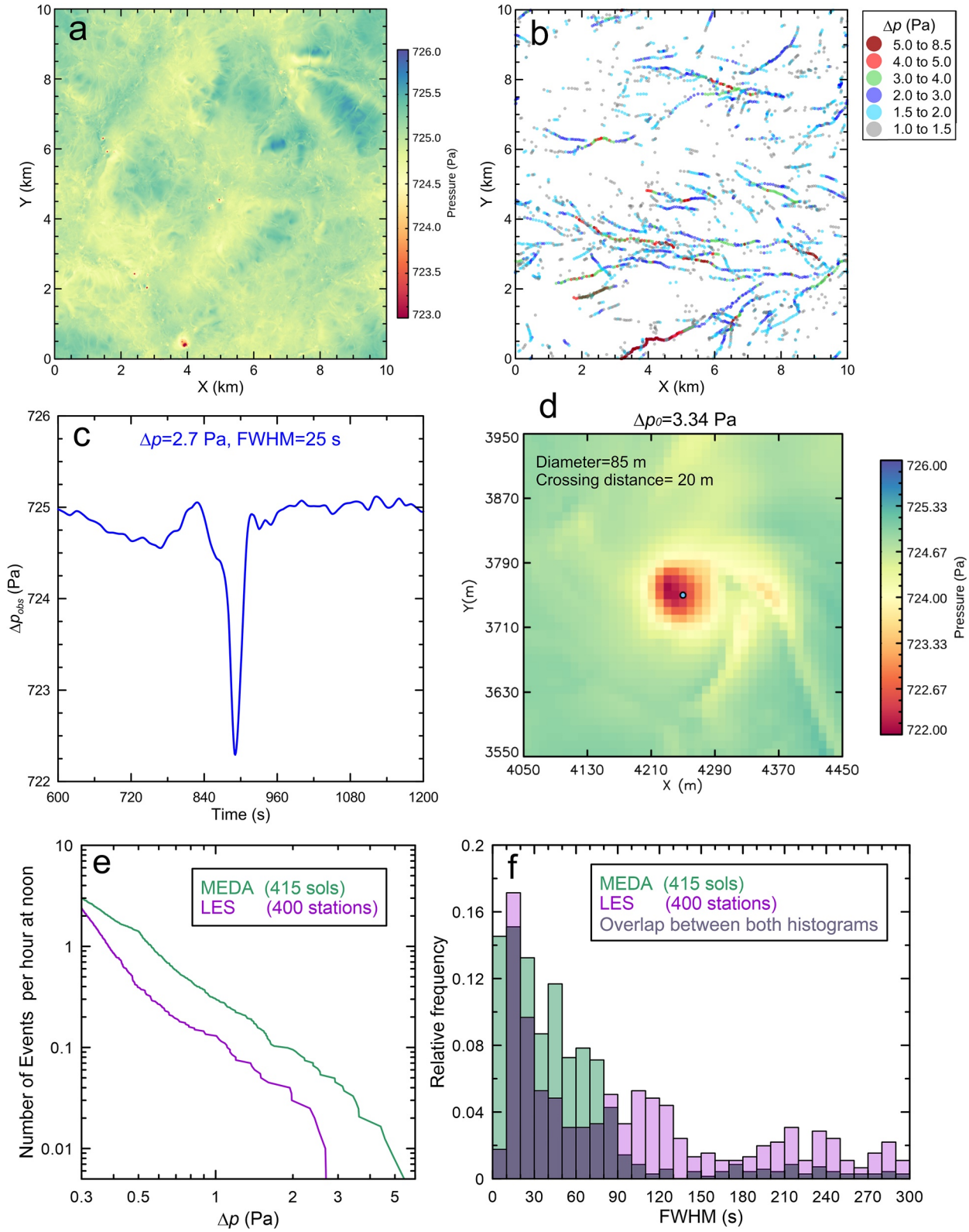

Figure 15. Large Eddy Simulation (LES) simulation of Jezero convective period at noon for $Ls = 45°$. (a) Snapshot of the pressure field in the simulation at 12:04 showing intense vortices. (b) Tracks of the most intense vortices over the time period 12:00–12:30. (c) Highest pressure drop identified by the Mars Environmental Dynamics Analyzer (MEDA) algorithm. (d) The same vortex in the LES with its true parameters. The position of the station recording this encounter is shown with a small dot in the center of the domain. The large pixels in this image correspond to the spatial resolution of 10 m in the simulation. (e) Comparison of the number of events per hour detected in MEDA data and LES at noon. (f) Relative frequency of both distributions as a function of the vortex detection Full Width at Half Maximum.

are never detected, or that are detected as weaker vortices because of the distance at which they approach one of the measurement points. Figure S8 in Supporting Information S1 shows some of the most intense vortices in the simulation and how they are perceived by the closest meteorological station.

A systematic comparison of our detections of MEDA vortices and those in the LES analysis is given in Figure 15e. For pressure drops larger than 0.5 Pa, MEDA detects three times as many events per hour at noon as in the simulation. The MEDA data also has stronger events than those found in the equivalent analysis of the LES. The most intense vortices found by MEDA at Jezero are comparable to the most intense vortices in the simulation (although these very intense vortices in the simulation are identified as weaker events by the synthetic stations, since those vortices have a small chance of passing very close to individual stations). The distribution of the duration of the events is similar for events of 20–30 s, and very different for short and long events (Figure 15f). This can be explained because short events cannot be examined in the LES, which is limited by its output frequency of 0.1 Hz and its spatial resolution of 10 m, and long duration events are weaker in intensity and in MEDA tend to be more turbulent. In the LES, distant and long-duration vortices are detected because of the clean pressure signal and the regular background winds imposed in the model. However, in the MEDA pressure data at Jezero, a measurement noise of 0.1 Pa combined with turbulent fluctuations in pressure (Sánchez-Lavega et al., 2022), variations in wind speed and direction (Rodriguez-Manfredi et al., 2023; Viúdez-Moreiras et al., 2022) make detections of distant events more difficult to detect. Additional factors, such as the variations in spatial scales of a few meters of terrain roughness, inclination, thermal inertia, and albedo might also contribute to produce a more turbulent atmosphere than the one that can be simulated by the LES.

The LES allows us to examine how many vortices are present at any given time, and in particular, how many intense vortices with the potential to become dusty are produced in the simulation. The probability of a vortex to be dusty at Jezero depends on the intensity of the pressure drop and becomes larger than 75% for events detected with $\Delta p_{obs} = 2.0$ Pa or more. Over the 1,800 s of the LES, there are 20 vortices active with pressure drops from 1.0 to 8.4 Pa with a mean pressure drop intensity of 2.0 Pa. This results in a vortex production rate in the simulation of at least 0.2 events km^{-2} at noon (with $\Delta p_{\mathrm{obs}} > 2.0$ Pa). Assuming that the MEDA observations and LES scale are linear, a factor difference of 3 between modeled and observed activity leads to a production rate of comparable vortices in MEDA data of 0.6 km^{-2} at noon. These events are nearly always dusty in MEDA data. In addition, the integrated vortex and DD activity over a sol can be 3–4 times larger than the peak activity at noon, scaling to a DD production rate at Jezero of ∼1.8–2.4 DD km^{-2} sol^{-1}. This estimation is in agreement with an independent estimation of the DD production rate at Jezero of 2.0 DD km^{-2} sol^{-1}, which is based on a combination of the frequency of DDs detected with the RDS Top detectors, the estimated diameters of vortices from the duration of RDS variations, the average winds, and the range of times the vortices are expected to be active (Toledo et al., 2023).

7. Discussion

7.1. Density of Dust Devils at Jezero

Our analysis of the LES illustrates the difficulties to observe the very close passages of vortices. In our model fit to selected MEDA vortices, we observed the close passages of several DDs at distances much smaller than the vortex radius. Statistically, these are infrequent events that produce intense pressure drops and that in our sample of MEDA vortices were DDs that carried significant amounts of dust. Here we investigate the statistical significance of these close passing DDs.

We model the trajectories of vortices randomly launched in a two-dimensional box of 10 km × 10 km assuming a vortex production rate, ρ_v, defined as the number of DDs per square kilometer and sol. We consider that vortices can survive active during a time $t_v = 0.66 \times (D)^{\frac{2}{3}}$, where, D is the vortex diameter and t_v is given in minutes (R. Lorenz, 2013; R. D. Lorenz, 2013). Vortices with diameters of 20–40 m survive 5–7.5 min and we assume a fixed surviving time of 7.5 min. We also assume a vortex drift of $V_v = 5$ ms^{-1} from average wind speeds measured during daytime at Jezero (Rodriguez-Manfredi et al., 2023). We examine trajectories replicating 415 sols of data with measurements for 50% of the time. The trajectory of each individual vortex is integrated over 7.5 min measuring its closest approach to the center of the model domain, regardless of any distribution of diameters. For each simulated sol we identify the closest approach to the center of the domain and we count how many vortices pass at a range of distances from 10 to 500 m. We perform 15–25 Monte Carlo simulations of the whole process

for each value of ρ_v to obtain statistical values (each Monte Carlo simulation implying the integration in time of $\rho_v \times 100$ km$^2 \times 415/2$ hr vortex trajectories).

The DD with the closest approach to Perseverance was the one in sol 82, with a modeled minimum approach of 0.15 m. To take into account possible uncertainties in the minimum distance of the modeled vortices, we consider that this minimum approach could be as high as 1.0 m. We examine our simulations to determine which DD production rate is compatible with this observation. Figure 16a shows a whisker plot of these simulations. In order to have a single vortex crossing a distance of Perseverance of 0.15–1.0 m, a DD production rate of 0.5–5.0 DD km^{-2}sol^{-1} is needed, with the best results found for 3.0 DD km^{-2}sol^{-1}. Smaller vortex survival times than the one assumed would require higher DD production rates.

Figure 16b shows the number of events in simulations with different production rates that cross at different distances to the MEDA sensors. This is compared with the number of vortices detected for different pressure drop thresholds. A DD production rate of 2.5 DDs km^{-2}sol^{-1} is compatible with detected pressure drops in MEDA data of 2.0 Pa (most of them being dusty at Jezero) being caused by more intense vortices crossing at distances of about 30 m or smaller. The very large number of vortices detected in MEDA with $\Delta p_{obs} > 0.5$ Pa cannot be fitted by this production rate, and requires the more frequent formation of vortices of smaller intensity. Thus, the production rate of small intensity vortices must be substantially larger than the 2.5 DDs km^{-2}sol^{-1} that we consider can fit the intense vortices that we detect with values of about 2.0 Pa and tends to be dusty.

In addition, there are three DDs in the MEDA observations with a diameter of 87–135 m crossing at distances of about 30 m. Figure 16c shows results of our Monte Carlo simulation of trajectories considering a DD production rate of DDs of this size category of 0.1 DD km^{-2}sol^{-1}. This simulation fits the number of encounters of large vortices at 30 m. Therefore, vortices with diameters of 100 m are produced at Jezero 25 times less frequently than the vortices that we detect with a mean diameter of 20 m.

When putting together our results, we find that for typical DD sizes of 20 m in diameter, DD production rates of 2.0–3.0 DD km^{-2}sol^{-1} are reasonable values. This range of values is comparable to other studies at Jezero (Toledo et al., 2023), and smaller than the largest values found at some other locations on Mars that range from 7 to 15 DD km^{-2}sol^{-1} from analysis of DD surveys in images obtained by Pathfinder cameras (Ferri et al., 2003; Metzger et al., 1999), to 50 DD km^{-2}sol^{-1} from Spirit during a season of high DD activity (Ls = 173°–340°) (Ferri et al., 2003; Greeley et al., 2006, 2010; Waller, 2011). In many other locations, like Gale crater, the DDs production rate is much smaller (Ordóñez-Etxeberria et al., 2020), or negligible, like in the location of InSight in Elysium Planitia (Spiga et al., 2021). While vortices in Jezero are very frequently dusty, the observed DD activity is not beyond what has been observed in the past.

7.2. Intense Vortices and Risks to Surface Hardware

The WS has two booms. Each boom is made of 6 transducer boards that include redundant elements. In each transducer board, hot and cold dices are connected to the board by sub-mm diameter filaments (Rodriguez-Manfredi et al., 2021). Over the course of the mission, two failures in the boards were detected at the same time as encounters with DDs on sols 313 and 413. The DD on sol 313 was the thirteenth dustiest event detected and the DD on sol 413 was the fourth dustiest. The characteristics of these events are summarized in Table 2. Other failures in different boards have also occurred in other moments without a direct contribution from DDs, and MEDA wind measurements obtained after sol 313 require a recalibration of the wind measurements not available at the time of this writing.

The first event occurred during the dust storm period and affected the WS boom 2. Figure S9 in Supporting Information S1 shows images of the WS and MEDA measurements obtained during passage of this DD. The delay between the peak pressure drop and the largest decrease in light measured by RDS Top 7 suggest this was not a direct impact with the vortex, but a more tangential one. Wind measurements obtained just before the WS failure peaked at values of 22 ms^{-1}, which are on the same level as the peak winds observed in the most intense vortices detected in the MEDA data set. All these factors suggest a vortex passage at a distance comparable to the vortex radius, which would be coincident with the strongest winds in the vortex. Using Equation (1) to invert the value of the central pressure drop, this would require a vortex with a central pressure drop of at least 7 Pa. If the vortex impacted Perseverance at a distance larger than its radius, then the DD could have been substantially more intense carrying larger size grains. Because we only have wind

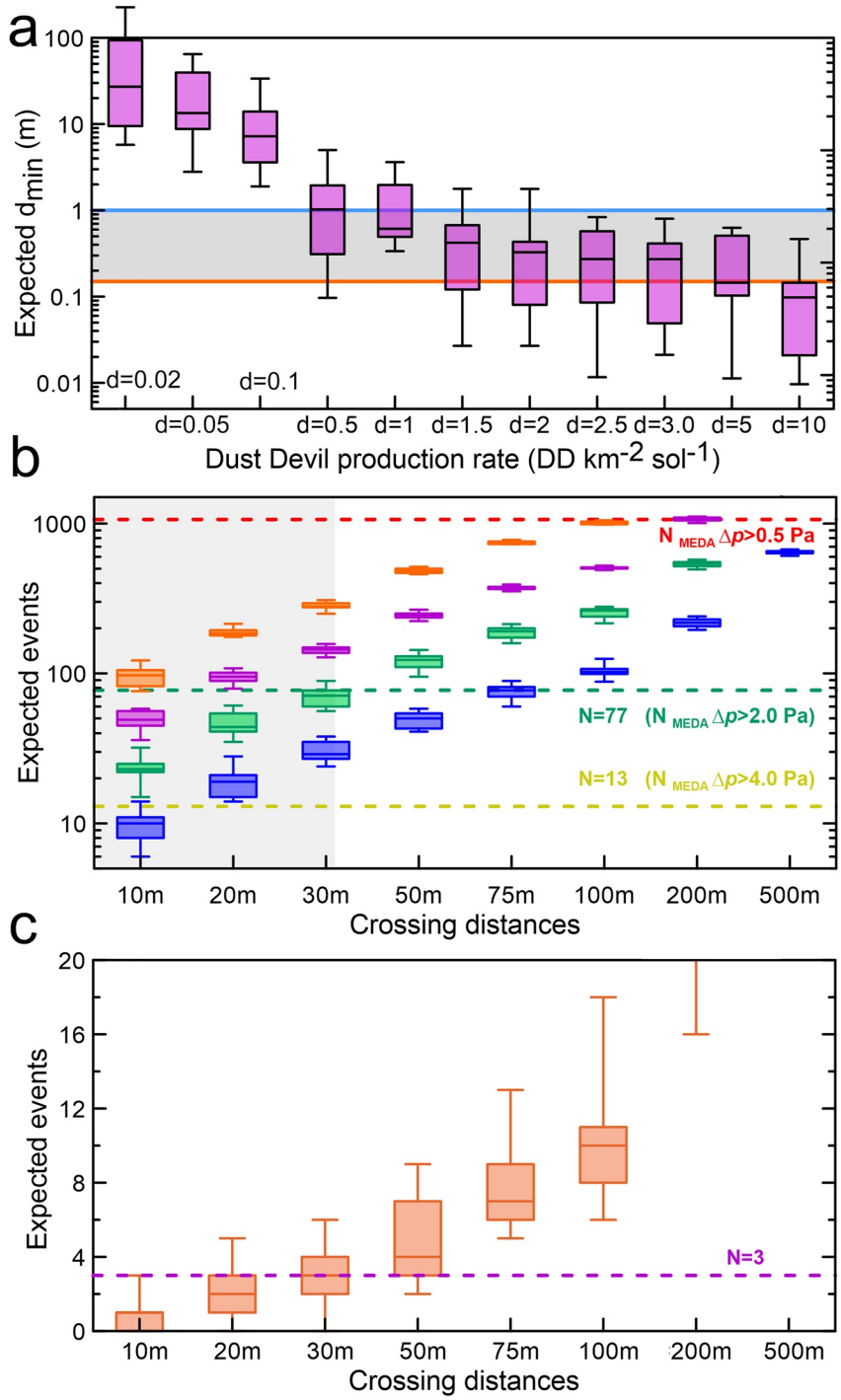

Figure 16. Monte Carlo simulations of trajectories for different dust devil (DD) production rates. (a) Whisker box plot of the minimum crossing distance of a population of vortices produced by Monte Carlo simulations with production rates of 0.02–10.0 DDs km^{-2} sol^{-1}. For each production rate, the box shows the distribution of values organized in quartiles with the median being the central horizontal line. Long horizontal lines show minimum distances of 0.15 and 1.0 m, and the dashed area is the region to fit. (b) Whisker box plot of the number of vortices that would cross at different minimum distances of Mars Environmental Dynamics Analyzer (MEDA) for values of ρ_v from 1.0 (blue), 2.5 (green), 5.0 (purple), and 10.0 (orange), all in units of DDs km^{-2}sol^{-1}. Horizontal lines show the number of detections in MEDA data of pressure drops with at least 4.0 Pa (yellow green), 2.0 Pa (green), and 0.5 Pa (red). (c) Whisker box plot of the number of vortices that would cross at minimum distances for $\rho_v = 0.1$ DDs km^{-2}sol^{-1}. The horizontal line highlights the three 100-m size DDs observed at a minimum distance of 30 m.

Table 2
Vortices Implied in Wind Sensors Damage

Sol	*Ls* (MY36)	LTST (hh:mm:ss)	Δp_{obs} (Pa)	Rank (Δp_{obs})	FWHM (s)	RDSTop7 (%)	Rank (RDSTop7)	WS peak (ms^{-1})
313	153.3	13:42:14	1.8	95	36	9	13	22
413	211.5	14:22:26	4.0	13	13	20	4	–

information during the approach phase, we cannot retrieve the physical parameters of this vortex using the vortex drift model.

The second WS failure that can be linked to a DD occurred on sol 413 and affected the WS boom 1. The event had a detected pressure drop of 4.0 Pa and a high dust content with a 20% reduction of irradiance measured by RDS. Although wind measurements were obtained during the vortex encounter, examining their values requires a new retrieval process that takes into account the functional boards at the time. Because the central pressure drop and event duration are typical of the very close approaches, and the dustiness of the vortex measured by RDS is high, we expect that this was a very close approach of an intense DD in Jezero with a likely size close to the most common vortices with diameters of $\sim 17 \pm 8$ m.

7.3. Contribution of Vortices to Dust-Lifting at Jezero

Greeley et al. (2006) computed the average dust flux to the atmosphere transported by DDs in Gusev crater from images obtained by the Spirit cameras. Vertical velocities in the DDs had a mean value of 1.8 ms^{-1}, and DDs transported an average dust flux of 2.1×10^{-5} kg m^{-2} s^{-1}. However this number could vary over several orders of magnitude for individual vortices and seasons.

MEDA offers information on the dust content of individual vortices from RDS data. However, its interpretation is subject to geometrical effects associated with the vortex size, crossing distance, and vortex path relative to the Sun. Thus, an unbiased quantification of how much dust each DD transports is not straight-forward. If we also consider the DD longevity relation from R. Lorenz (2013) and R. D. Lorenz (2013), then, the largest DD in the MEDA observations, that is, the DD on sol 213 with a 135 m diameter, can lift 45% of all the dust lifted by the 22 events that we have fitted.

If we assume for estimative purposes that the very uncertain average values of vertical velocity and dust flux found at Gusev crater by Greeley et al. (2006) may also be used for Jezero, then the vortex on sol 213 could potentially raise 300 kg of dust to the atmosphere over a life time of 1,000 s. If vortices at Jezero have a mean diameter of 17 m, as calculated from the closest passing vortices, that means that individual vortices can lift about 1.4 kg of dust each. A DD production rate of events of this size of 2.5 DD km^{-2} sol^{-1} would result in a dust flux of 3.5 kg km^{-2} sol^{-1}, which is about 20% of the estimates at Gusev crater from Greeley et al. (2006).

The large vortices with sizes of 100 m and a production rate of 0.1 DD km^{-2} sol^{-1} would result in longer-lived vortices with a dust flux of 16 kg km^{-2} sol^{-1}. This means that large vortices dominate the dust flux at Jezero, even though a full calculation of how much dust is being lifted by vortices is not possible with the current data.

8. Conclusions

The rich vortex and DD activity at Jezero, and the multiple atmospheric sensors in MEDA, combine to provide a valuable description of vortices and DDs on Mars. Our main findings in examining these data are:

- Vortices are abundant in Jezero during daytime hours. Their average abundance from analysis of pressure data is 4.9 vortices per sol with a $\Delta p_{obs} > 0.5$ Pa. This number takes into account a renormalization for the portion of time over which MEDA operates. One in every five of these vortices carries dust. The daily activity of vortices and DDs peaks at noon with 1.1 vortices per hour with $\Delta p_{obs} > 0.5$ Pa and 0.25 DDs per hour.
- Nighttime pressure drops similar to those caused by daytime vortices are rare but do exist. Some cases can be caused by convective plumes from the RTG and are accompanied by high temperatures. Other cases do not seem related with the RTG and should be caused by the environment. Additional long pressure drops are observed during the day and can be highly variable, potentially indicative of the passage of convective cells.

- The seasonal evolution of vortices and DDs over $Ls = 6°–213°$ is small, but there are clear changes at the end of the Summer and early Autumn with a more spread activity in local time of sol that preserves an overall vortex activity of 4–5 vortices per sol. The seasonal variation of vortices occurs in parallel to changes in the vertical thermal gradient of the atmosphere, which is small until the arrival of the Autumn (Munguira et al., 2023).
- DDs became very frequent during the first sols of a dust storm that affected Jezero at $Ls = 152°$. These sols had warmer air temperatures and lower surface to air temperature differences than in previous sols. Vortex activity was inhibited a few sols later accompanying a reduction in the temperature of the air and surface with a gradual increase to the seasonal vertical thermal gradient.
- There is a strong correlation between the intensity of the vortex from the detected pressure drop, and its dust content. Most of the vortices with $\Delta p > 2.0$ Pa were dusty. The strongest decrease in RDS Top 7 was caused by a long and intense pressure drop that resulted in a light reduction of 26% ($\Delta\tau$ increase of 0.3). This was caused by a close encounter at 30 m of a DD with a diameter of 135 m.
- Clusters of vortices and DDs are related to the terrain properties. The most intense vortices are found over terrains with relatively low thermal inertia (TI $\approx$ 300), which produce high thermal gradients at near noon hours. There is a strong correlation between the local vertical thermal gradient and the intensity of the vortices. However, some intense and large vortices are found over terrains with relatively high thermal inertia and small vertical thermal gradients. We suggest that these events could have formed over different terrains and moved over the location where they are detected. Low thermal inertia terrains are generally dust covered, favoring DD formation in the same locations where intense vortices are formed.
- A comparison of vortex activity at Jezero with a LES calculated for $Ls = 45°$ shows similar characteristics, although MEDA measurements of vortex activity suggest three times higher activity at Jezero than the simulation. The LES allows to examine biases from a meteorological station that has a low probability of finding very close events. The comparison of MEDA data and the LES suggests a DD production rate of 1.8–2.4 DD km^{-2} sol^{-1}.
- MEDA pressure and wind data allow us to fit models of vortices that were applied over DDs causing intense pressure drops. These fits result in vortex diameters from 5 to 135 m. The DDs with the closest trajectories to Perseverance have a mean diameter of 17 m and the mean diameter of all vortices that we could fit to models was 34 m. Model fits predict that at least one of the vortices detected had a central pressure drop of 9.0 Pa, similar to the most intense vortices observed at Elysium Planitia (Spiga et al., 2021).
- The abundance of DDs passing Perseverance at very close distances results in a vortex formation rate at Jezero of 2.0–3.0 DDs km^{-2} sol^{-1}. A comparison of this formation rate with the number of vortices detected in MEDA data suggests that vortices with pressure drops of 2.0 Pa, which are generally dusty, correspond to the approach of stronger vortices observed at a distance that in most cases is smaller than 30 m.
- At least three large DDs with diameters of 100 m passed within 30 m of Perseverance. This implies a vortex formation rate for events of this size of 0.1 DDs km^{-2} sol^{-1}. The comparison with the formation rate of smaller DDs implies that the total dust lifting by vortices at Jezero is dominated by the activity of the larger vortices.
- Two DDs were responsible for damaging part of the hardware of the MEDA WSs. These sensors contain fragile elements such as sub-mm wide conducting filaments exposed to the Martian atmosphere. Since DDs are common features over most of the surface of Mars new missions may have to take into account the risks of impacts by sand particles or mm-size granules at speeds of $\sim$15−25 ms^{-1}.

Convective vortices in Jezero seem to be able to raise dust much more efficiently than in locations such as Elysium and Gale crater, where InSight and MSL have found no dust lifting activity (InSight), or very low dust liftting activity (MSL). The dust lifting activity by DDs at Jezero is probably smaller than the dust lifting at Gusev crater observed by Spirit, but in most of these missions, observations over different MYs have found strong differences. Thus, new observations by Perseverance over different seasons and terrains, exploring properties such as surface roughness, particle size, and cohesion from surface images, will help to understand the characteristics that make Jezero so active in developing DDs within its rich population of convective vortices.

Data Availability Statement

The Mars Environmental Dynamics Analyzer (MEDA) data used in this study is available via de Planetary Data System in de la Torre Juarez & Rodriguez-Manfredi (2021). Derived products include a catalog of pressure drops, a catalog of vortices and dust devils with additional environmental data, a summary of the event modeled and

their physical parameters and a movie showing the evolution of pressure in the LES presented in Section 6. These data sets are available in Hueso et al. (2022). The programs used for this analysis are written in IDL and Fortran and are publicly available in Hueso (2022).

Acknowledgments
The authors are very grateful to the entire Mars 2020 science operations team. The authors would also like to thank Lori Fenton and an anonymous reviewer for many suggestions that greatly improved the manuscript. This work was supported by Grant PID2019-109467GB-I00 funded by MCIN/AEI/10.13039/501100011033/ and by Grupos Gobierno Vasco IT1742-22 and by the Spanish National Research, Development and Innovation Program, through the Grants RTI2018-099825-B-C31, ESP2016-80320-C2-1-R, and ESP2014-54256-C4-3-R. Baptiste Chide is supported by the Director's Postdoctoral Fellowship from the Los Alamos National Laboratory. M. Lemmon is supported by contract 15-712 from Arizona State University and 1607215 from Caltech-JPL. R. Lorenz was supported by JPL contract 1655893. Germán Martínez acknowledges JPL funding from USRA Contract Number 1638782. A. Munguira was supported by Grant PRE2020-092562 funded by MCIN/AEI and by "ESF Investing in your future." A. Vicente-Retortillo is supported by the Spanish State Research Agency (AEI) Project No. MDM-2017-0737 Unidad de Excelencia "María de Maeztu"-Centro de Astrobiología (INTA-CSIC), and by the Comunidad de Madrid Project S2018/NMT-4291 (TEC2SPACE-CM). Part of the research was carried out at the Jet Propulsion Laboratory, California Institute of Technology, under a contract with the National Aeronautics and Space Administration (80NM0018D0004). Finnish researchers acknowledge the Academy of Finland Grant 328 310529. Researchers based in France acknowledge support from the CNES for their work on Perseverance.

References

Apestigue, V., Gonzalo, A., Jiménez, J., Boland, J., Lemmon, M., de Mingo, J., et al. (2022). Radiation and dust sensor for Mars environmental dynamic analyzer onboard M2020 rover. *Sensors*, *22*(8), 2907. https://doi.org/10.3390/s22082907

Balme, M., & Greeley, R. (2006). Dust devils on Earth and Mars. *Reviews of Geophysics*, *44*(3), RG3003. https://doi.org/10.1029/2005RG000188

Banfield, D., Spiga, A., Newman, C., Forget, F., Lemmon, M., Lorenz, R., et al. (2020). The atmosphere of Mars as observed by InSight. *Nature Geoscience*, *13*(3), 190–198. https://doi.org/10.1038/s41561-020-0534-0

Basu, S., Richardson, M. I., & Wilson, R. J. (2004). Simulation of the Martian dust cycle with the GFDL Mars GCM. *Journal of Geophysical Research*, *109*(E11), E11006. https://doi.org/10.1029/2004JE002243

Chatain, A., Spiga, A., Banfield, D., Forget, F., & Murdoch, N. (2021). Seasonal variability of the daytime and nighttime atmospheric turbulence experienced by InSight on Mars. *Geophysical Research Letters*, *48*(22), e95453. https://doi.org/10.1029/2021GL095453

de la Torre Juarez, M., & Rodriguez-Manfredi, J. A. (2021). *Mars 2020 MEDA bundle*. NASA Planetary Data System. https://doi.org/10.17189/1522849

Ellehoj, M. D., Gunnlaugsson, H. P., Taylor, P. A., Kahanpää, H., Bean, K. M., Cantor, B. A., et al. (2010). Convective vortices and dust devils at the Phoenix Mars mission landing site. *Journal of Geophysical Research*, *115*(E8), E00E16. https://doi.org/10.1029/2009JE003413

Farley, K. A., Williford, K. H., Stack, K. M., Bhartia, R., Chen, A., de la Torre, M., et al. (2020). Mars 2020 mission overview. *Space Science Reviews*, *216*(8), 142. https://doi.org/10.1007/s11214-020-00762-y

Fenton, L., Reiss, D., Lemmon, M., Marticorena, B., Lewis, S., & Cantor, B. (2016). Orbital observations of dust lofted by daytime convective turbulence. *Space Science Reviews*, *203*(1–4), 89–142. https://doi.org/10.1007/s11214-016-0243-6

Fergason, R. L., Christensen, P. R., & Kieffer, H. H. (2006). High-resolution thermal inertia derived from the Thermal Emission Imaging System (THEMIS): Thermal model and applications. *Journal of Geophysical Research*, *111*(E12), E12004. https://doi.org/10.1029/2006JE002735

Ferri, F., Smith, P. H., Lemmon, M., & Rennó, N. O. (2003). Dust devils as observed by Mars Pathfinder. *Journal of Geophysical Research*, *108*(E12), 5133. https://doi.org/10.1029/2000JE001421

Gómez-Elvira, J., Armiens, C., Castañer, L., Domínguez, M., Genzer, M., Gómez, F., et al. (2012). REMS: The environmental sensor suite for the Mars Science Laboratory rover. *Space Science Reviews*, *170*(1–4), 583–640. https://doi.org/10.1007/s11214-012-9921-1

Greeley, R., Waller, D. A., Cabrol, N. A., Landis, G. A., Lemmon, M. T., Neakrase, L. D. V., et al. (2010). Gusev Crater, Mars: Observations of three dust devil seasons. *Journal of Geophysical Research*, *115*(E8), E00F02. https://doi.org/10.1029/2010JE003608

Greeley, R., Whelley, P. L., Arvidson, R. E., Cabrol, N. A., Foley, D. J., Franklin, B. J., et al. (2006). Active dust devils in Gusev crater, Mars: Observations from the Mars exploration rover spirit. *Journal of Geophysical Research*, *111*(E12), E12S09. https://doi.org/10.1029/2006JE002743

Guzewich, S. D., Lemmon, M., Smith, C. L., Martínez, G., de Vicente-Retortillo, Á., Newman, C. E., et al. (2019). Mars Science Laboratory Observations of the 2018/Mars year 34 global dust storm. *Geophysical Research Letters*, *46*(1), 71–79. https://doi.org/10.1029/2018GL080839

Hueso, R. (2022). *General tools for analysis of convective vortices (IDL and Fortran Codes, version 0.9)*. Zenodo. https://doi.org/10.5281/zenodo.6958141

Hueso, R., Newman, C., del Río-Gaztelurrutia, T., Munguira, A., Sánchez-Lavega, A., Toledo, D., et al. (2022). Catalog of pressure drops, vortices and dust devils on Jezero crater, Mars, Ls = 6–213 plus large eddy simulation movie. *Zenodo*. https://doi.org/10.5281/zenodo.7315863

Jackson, B. (2022a). Estimating the heights of Martian vortices from Mars 2020 MEDA data. *Planetary Science Journal*, *3*(8), 203. https://doi.org/10.3847/PSJ/ac87f3

Jackson, B. (2022b). Vortices and dust devils as observed by the Mars environmental dynamics analyzer instruments on board the Mars 2020 perseverance rover. *Planetary Science Journal*, *3*(1), 20. https://doi.org/10.3847/PSJ/ac4586

Jackson, B., Crevier, J., Szurgot, M., Battin, R., Perrin, C., & Rodriguez, S. (2021). Inferring vortex and dust devil statistics from InSight. *Planetary Science Journal*, *2*(5), 206. https://doi.org/10.3847/PSJ/ac260d

Kahanpää, H., & Viúdez-Moreiras, D. (2021). Modelling Martian dust devils using in-situ wind, pressure, and UV radiation measurements by Mars. *Science Laboratory*, *359*, 114207. https://doi.org/10.1016/j.icarus.2020.114207

Kahre, M. A., Murphy, J. R., & Haberle, R. M. (2006). Modeling the Martian dust cycle and surface dust reservoirs with the NASA Ames general circulation model. *Journal of Geophysical Research*, *111*(E6), E06008. https://doi.org/10.1029/2005JE002588

Kahre, M. A., Murphy, J. R., Newman, C. E., Wilson, R. J., Cantor, B. A., Lemmon, M. T., & Wolff, M. J. (2017). The Mars dust cycle. In R. M. Haberle, R. T. Clancy, F. Forget, M. D. Smith, & R. W. Zurek (Eds.), *Asteroids, Comets, Meteors – ACM2017* (pp. 229–294). https://doi.org/10.1017/9781139060172.010

Kurgansky, M. V., Lorenz, R. D., Renno, N. O., Takemi, T., Gu, Z., & Wei, W. (2016). Dust devil steady-state structure from a fluid dynamics perspective. *Space Science Reviews*, *203*(1–4), 209–244. https://doi.org/10.1007/s11214-016-0281-0

Lemmon, M. T., Smith, M. D., Viudez-Moreiras, D., de la Torre-Juarez, M., Vicente-Retortillo, A., Munguira, A., et al. (2022). Dust, sand, and winds within an active Martian storm in Jezero crater. *Geophysical Research Letters*, *49*, e2022GL100126. https://doi.org/10.1029/2022GL100126

Lorenz, R. (2013). The longevity and aspect ratio of dust devils: Effects on detection efficiencies and comparison of landed and orbital imaging at Mars. *Icarus*, *226*(1), 964–970. https://doi.org/10.1016/j.icarus.2013.06.031

Lorenz, R. D. (2013). Irregular dust devil pressure drops on Earth and Mars: Effect of cycloidal tracks. *Planetary and Space Science*, *76*, 96–103. https://doi.org/10.1016/j.pss.2013.01.001

Lorenz, R. D. (2016). Heuristic estimation of dust devil vortex parameters and trajectories from single-station meteorological observations: Application to InSight at Mars. *Icarus*, *271*, 326–337. https://doi.org/10.1016/j.icarus.2016.02.001

Lorenz, R. D., Lemmon, M. T., & Maki, J. (2021). First Mars year of observations with the InSight solar arrays: Winds, dust devil shadows and dust accumulation. *Icarus*, *364*, 114468. https://doi.org/10.1016/j.icarus.2021.114468

Lorenz, R. D., & Reiss, D. (2015). Solar panel clearing events, dust devil tracks, and in-situ vortex detections on Mars. *Icarus*, *248*, 162–164. https://doi.org/10.1016/j.icarus.2014.10.034

Martínez, G. M., Sebastián, E., Vicente-Retortillo, A., Smith, M. D., Johnson, J. R., Fischer, E., et al. (2023). Surface energy budget, albedo and thermal inertia at Jezero crater, Mars, as observed from the Mars 2020 MEDA instrument. *Journal of Geophysical Research: Planets*, *128*, e2022JE007537. https://doi.org/10.1029/2022JE007537

Martínez, G. M., Vicente-Retortillo, A., Vasavada, A. R., Newman, C. E., Fischer, E., Rennó, N. O., et al. (2021). The surface energy budget at Gale crater during the first 2500 sols of the Mars Science Laboratory mission. *Journal of Geophysical Research: Planets*, *126*(9), e06804. https://doi.org/10.1029/2020JE006804

Mason, J. P., Patel, M. R., & Lewis, S. R. (2013). Radiative transfer modelling of dust devils. *Icarus*, *223*(1), 1–10. https://doi.org/10.1016/j.icarus.2012.11.018

Metzger, S. M., Carr, J. R., Johnson, J. R., Parker, T. J., & Lemmon, M. T. (1999). Dust devil vortices seen by the Mars Pathfinder Camera. *Geophysical Research Letters*, *26*(18), 2781–2784. https://doi.org/10.1029/1999GL008341

Munguira, A., Hueso, R., Sánchez-Lavega, A., de la Torre-Juarez, M., Martínez, G., Newman, C. E., et al. (2023). Near surface atmospheric temperatures at Jezero from Mars 2020 MEDA measurements. *Journal of Geophysical Research: Planets*, *128*, e2022JE007559. https://doi.org/10.1029/2022JE007559

Murdoch, N., Stott, A., Gillier, M., Hueso, R., Lemmon, M., Martínez, G., et al. (2022). The sound of a Martian dust devil. *Nature Communications*, *13*(1), 7505. https://doi.org/10.1038/s41467-022-35100-z

Murphy, J., Steakley, K., Balme, M., Deprez, G., Esposito, F., Kahanpää, H., et al. (2016). Field measurements of terrestrial and Martian dust devils. *Space Science Reviews*, *203*(1–4), 39–87. https://doi.org/10.1007/s11214-016-0283-y

Neakrase, L. D. V., Balme, M. R., Esposito, F., Kelling, T., Klose, M., Kok, J. F., et al. (2016). Particle lifting processes in dust devils. *Space Science Reviews*, *203*(1–4), 347–376. https://doi.org/10.1007/s11214-016-0296-6

Newman, C. E., de la Torre Juárez, M., Pla-García, J., Wilson, R. J., Lewis, S. R., Neary, L., et al. (2021). Multi-model meteorological and aeolian predictions for Mars 2020 and the Jezero crater region. *Space Science Reviews*, *217*(1), 20. https://doi.org/10.1007/s11214-020-00788-2

Newman, C. E., Hueso, R., Lemmon, M. T., Munguira, A., Vicente-Retortillo, Á., Apestigue, V., et al. (2022). The dynamic atmospheric and aeolian environment of Jezero crater, Mars. *Science Advances*, *8*(21), eabn3783. https://doi.org/10.1126/sciadv.abn3783

Newman, C. E., Lewis, S. R., Read, P. L., & Forget, F. (2002). Modeling the Martian dust cycle, 1. Representations of dust transport processes. *Journal of Geophysical Research*, *107*(E12), 5123–6-18. https://doi.org/10.1029/2002JE001910

Ordonez-Etxeberria, I., Hueso, R., & Sánchez-Lavega, A. (2018). A systematic search of sudden pressure drops on Gale crater during two Martian years derived from MSL/REMS data. *Icarus*, *299*, 308–330. https://doi.org/10.1016/j.icarus.2017.07.032

Ordóñez-Etxeberria, I., Hueso, R., & Sánchez-Lavega, A. (2020). Strong increase in dust devil activity at Gale crater on the third year of the MSL mission and suppression during the 2018. *Global Dust Storm*, *347*, 113814. https://doi.org/10.1016/j.icarus.2020.113814

Pla-Garcia, J., Munguira, A., Newman, C., Bertrand, T., Martinez, G., Hueso, R., et al. (2022). Nocturnal turbulence at Jezero crater, as determined from MEDA measurements and modeling. *Earth and Space Science Open Archive*, 20. https://doi.org/10.1002/essoar.10512563.1

Putzig, N. E., & Mellon, M. T. (2007). Apparent thermal inertia and the surface heterogeneity of Mars. *Icarus*, *191*(1), 68–94. https://doi.org/10.1016/j.icarus.2007.05.013

Rafkin, S., Jemmett-Smith, B., Fenton, L., Lorenz, R., Takemi, T., Ito, J., & Tyler, D. (2016). Dust devil formation. *Space Science Reviews*, *203*(1–4), 183–207. https://doi.org/10.1007/s11214-016-0307-7

Reiss, D., Fenton, L., Neakrase, L., Zimmerman, M., Statella, T., Whelley, P., et al. (2016). Dust devil tracks. *Space Science Reviews*, *203*(1–4), 143–181. https://doi.org/10.1007/s11214-016-0308-6

Rennó, N. O., Burkett, M. L., & Larkin, M. P. (1998). A simple thermodynamical theory for dust devils. *Journal of the Atmospheric Sciences*, *55*(21), 3244–3252. https://doi.org/10.1175/1520-0469(1998)055<3244:asttfd>2.0.co;2

Richardson, M. I., Toigo, A. D., & Newman, C. E. (2007). PlanetWRF: A general purpose, local to global numerical model for planetary atmospheric and climate dynamics. *Journal of Geophysical Research*, *112*(E9), E09001. https://doi.org/10.1029/2006JE002825

Rodriguez-Manfredi, J. A., de la Torre Juárez, M., Alonso, A., Apéstigue, V., Arruego, I., Atienza, T., et al. (2021). The Mars environmental dynamics analyzer, MEDA. A suite of environmental sensors for the Mars 2020 mission. *Space Science Reviews*, *217*(3), 1–86. https://doi.org/10.1007/s11214-021-00816-9

Rodriguez-Manfredi, J. A., de la Torre Juárez, M., Sánchez-Lavega, A., Hueso, R., Martínez, G., Lemmon, M. T., et al. (2023). The diverse meteorology of Jezero crater over the first 250 sols of perseverance on Mars. *Nature Geoscience*, *16*, 19–28. https://doi.org/10.1038/s41561-022-01084-0

Ryan, J. A. (1972). Relation of dust devil frequency and diameter to atmospheric temperature. *Journal of Geophysical Research*, *77*(36), 7133–7137. https://doi.org/10.1029/JC077i036p07133

Ryan, J. A., & Lucich, R. D. (1983). Possible dust devils, vortices on Mars. *Journal of Geophysical Research*, *88*(C15), 11005–11011. https://doi.org/10.1029/JC088iC15p11005

Sánchez-Lavega, A., del Rio-Gaztelurrutia, T., Hueso, R., de la Torre-Juárez, M., Martínez, G. M., Harri, A.-M., et al. (2022). Mars 2020 Perseverance rover studies of the Martian atmosphere over Jezero from pressure measurements. *Journal of Geophysical Research: Planets*, *128*, e2022JE007480. https://doi.org/10.1029/2022JE007480

Spiga, A., Murdoch, N., Lorenz, R., Forget, F., Newman, C., Rodriguez, S., et al. (2021). A study of daytime convective vortices and turbulence in the Martian planetary boundary layer based on half-a-year of InSight atmospheric measurements and large-eddy simulations. *Journal of Geophysical Research: Planets*, *126*(1), e06511. https://doi.org/10.1029/2020JE006511

Toledo, D., Apéstigue, V., Arruego, I., Lemmon, M., Gómez, L., Montoro, A. d. F., et al. (2023). Dust devil frequency of occurrence and radiative effects at Jezero crater, Mars, as measured by MEDA Radiation and Dust Sensor (RDS). *Journal of Geophysical Research: Planets*, *128*, e2022JE007494. https://doi.org/10.1029/2022JE007494

Vicente-Retortillo, Á., Martínez, G. M., Renno, N., Newman, C. E., Ordonez-Etxeberria, I., Lemmon, M. T., et al. (2018). Seasonal deposition and lifting of dust on Mars as observed by the Curiosity rover. *Scientific Reports*, *8*(1), 17576. https://doi.org/10.1038/s41598-018-35946-8

Viúdez-Moreiras, D., Lemmon, M., Newman, C. E., Guzewich, S., Mischna, M., Gómez-Elvira, J., et al. (2022). Winds at the Mars 2020 landing site: 1. Near-surface wind patterns at Jezero crater. *Journal of Geophysical Research: Planets*, *127*, e2022JE007522. https://doi.org/10.1029/2022JE007522

Viúdez-Moreiras, D., Newman, C. E., Forget, F., Lemmon, M., Banfield, D., Spiga, A., et al. (2020). Effects of a large dust storm in the near-surface atmosphere as measured by InSight in Elysium Planitia, Mars. Comparison with Contemporaneous measurements by Mars Science Laboratory. *Journal of Geophysical Research: Planets*, *125*(9), e06493. https://doi.org/10.1029/2020JE006493

Waller, D. (2011). *Active dust devils on mars: A comparison of six spacecraft landing sites*. Arizona State University.

Wu, Z., Richardson, M. I., Zhang, X., Cui, J., Heavens, N. G., Lee, C., et al. (2021). Large eddy simulations of the dusty Martian convective boundary layer with MarsWRF. *Journal of Geophysical Research: Planets*, *126*(9), e06752. https://doi.org/10.1029/2020JE006752